Functional characterization of the disease-associated *CCL2* rs1024611G-rs13900T haplotype: The role of the RNA-binding protein HuR

Feroz Akhtar[1], Joselin Hernandez Ruiz[2], Ya-Guang Liu[3], Roy G. Resendez[1], Denis Feliers[4‡], Liza D. Morales[5], Alvaro Diaz-Badillo[1], Donna M. Lehman[1], Rector Arya[1], Juan Carlos Lopez-Alvarenga[6], John Blangero[5], Ravindranath Duggirala[1], and Srinivas Mummidi[1]*

[1]Department of Health and Behavioral Sciences, Texas A&M University- San Antonio, Texas, USA, [2] Utah Center for Genetic Discovery, Department of Human Genetics, University of Utah, Salt Lake City, Utah, USA, [3]Department of Pathology, School of Medicine, University of Texas Health San Antonio, San Antonio, Texas, USA, [4]Department of Medicine, School of Medicine, University of Texas Health San Antonio, San Antonio, Texas, USA, [5] South Texas Diabetes and Obesity Institute, Department of Genetics, School of Medicine, University of Texas Rio Grande Valley, Brownsville, Texas, USA, [6]Department of Population Health and Biostatistics, School of Medicine, University of Texas Rio Grande Valley, Harlingen, Texas, USA,

[‡]Current Address: Novartis Institute for Biomedical Research San Diego, San Diego, CA.

* **CORRESPONDING AUTHOR:**

Srinivas Mummidi, D.V.M., Ph.D.

Email: srinivas.mummidi@tamusa.edu

Abstract

CC-chemokine ligand 2 (CCL2) is involved in the pathogenesis of several diseases associated with monocyte/macrophage recruitment, such as HIV-associated neurocognitive disorder (HAND), tuberculosis, and atherosclerosis. The rs1024611 (alleles: A>G; G is the risk allele) polymorphism in the *CCL2 cis*-regulatory region is associated with increased CCL2 expression in vitro and ex vivo, leukocyte mobilization in vivo, and deleterious disease outcomes. However, the molecular basis for the rs1024611-associated differential CCL2 expression remains poorly characterized. It is conceivable that genetic variant(s) in linkage disequilibrium (LD) with rs1024611 could mediate such effects. Previously, we used rs13900 (alleles: C>T) in the *CCL2* 3' untranslated region (3' UTR) that is in perfect LD with rs1024611 to demonstrate allelic expression imbalance (AEI) of *CCL2* in heterozygous individuals. Here we tested the hypothesis that the rs13900 could modulate *CCL2* expression by altering mRNA turnover and/or translatability. The rs13900 T allele conferred greater stability to the *CCL2* transcript when compared to the rs13900 C allele. The rs13900 T allele also had increased binding to Human Antigen R (HuR), an RNA-binding protein, in vitro and ex vivo. The rs13900 alleles imparted differential activity to reporter vectors and influenced the translatability of the reporter transcript. We further demonstrated the role of HuR in mediating allele-specific effects on CCL2 expression in overexpression and silencing studies. Our studies suggest that the differential interactions of HuR with rs13900 could modulate CCL2 expression and could in part explain the interindividual differences in CCL2-mediated disease susceptibility.

54 **Introduction**

55 Identification of functional and/or causal genetic variants continues to pose a significant
56 challenge in the post-genome-wide association studies (post-GWAS) era (MacArthur et al.,
57 2017; Tam et al., 2019; Visscher et al., 2017). While emphasis has been placed on
58 polymorphisms that map to *cis*-elements in enhancers and promoters, genetic variants that
59 disrupt cis-elements in RNA binding protein (RBP) motifs in 3' UTR have received much less
60 attention. For many genes, the interactions of their 3' UTRs with specific stabilizing and
61 destabilizing RBPs play a critical role in modulating post-transcriptional events such as mRNA
62 turnover and translatability (Mayr, 2019; Schwerk and Savan, 2015). The lack of a mechanistic
63 understanding of how SNPs localizing to RBP motifs could impact gene expression impedes
64 a greater understanding of the variability in disease susceptibility and outcomes.

65

66 Post-transcriptional mechanisms are thought to play a crucial role in the initiation and
67 resolution of the inflammatory response (Anderson, 2010; Yoshinaga and Takeuchi, 2019).
68 Such regulation can profoundly affect gene expression levels; modest changes in mRNA
69 stability can lead to significant effects on mRNA and protein abundance (Buccitelli and
70 Selbach, 2020; Ross, 1995). Notably, a genome-scale study using mouse dendritic cells
71 demonstrated that post-transcriptional mRNA degradation was a salient feature of
72 inflammatory and immune signaling genes, as well as targets of NF-kappaB signaling following
73 lipopolysaccharide (LPS) stimulation (Rabani et al., 2011). In addition, polymorphisms in non-
74 coding regions such as the 3' UTR can have a significant impact on mRNA stability and
75 translatability. For example**,** a genome-wide study of variation in gene-specific mRNA decays
76 in lymphoblastoid cell lines across individuals found about 195 genetic variants that are
77 specifically associated with variation in mRNA decay rates, called "rdQTLs" (RNA Decay
78 Quantitative Trait Loci) (Pai et al., 2012). The authors estimated that 35% of the most
79 significant eQTL (Expression Quantitative Trait Loci) single nucleotide polymorphisms (SNPs)
80 are associated with decay rates (Pai et al., 2012). In another study, Duan *et al*. reported that
81 ~37% of gene expression differences among individuals may be attributed to RNA half-life

82 differences (Duan et al., 2013). Farh et al., reported that the 3' UTRs are highly enriched for
83 eQTL candidate causal SNPs (>1,500) relative to other transcribed SNPs (Farh et al., 2015).
84 However, the molecular mechanisms by which these polymorphisms alter mRNA stability or
85 translatability are poorly understood.
86
87 CCL2 is a potent monocyte chemoattractant produced by various cell types, either
88 constitutively or following activation. CCL2 expression can be regulated by inflammatory
89 molecules (e.g., IL-1, TNFα, LPS, and IFNγ) and growth factors (e.g., PDGF). While the cells
90 of monocyte-macrophage lineage are a major source of CCL2 (Yoshimura et al., 1989), other
91 cell types, such as fibroblasts, astrocytes, epithelial, and endothelial cells, also are an
92 important source (Deshmane et al., 2009). CCL2 mediates recruitment of monocytes, memory
93 T-cells, and dendritic cells to the site of inflammation (Gschwandtner, Derler and Midwood,
94 2019; Melgarejo et al., 2009) and there is substantial evidence implicating CCL2 as a key
95 mediator in macrophage-mediated diseases. Rovin et al. described a SNP in the 5'-regulatory
96 region of *CCL2* annotated as rs1024611 (dbSNP database; originally designated as –
97 2518A>G (Rovin, Lu and Saxena, 1999) or –2578A>G (Gonzalez et al., 2002)) that was
98 associated with increased plasma CCL2 expression (Rovin, Lu and Saxena, 1999). This SNP
99 is associated with increased serum CCL2 levels, enhanced macrophage recruitment to
100 tissues, and progression to HIV-associated dementia (Gonzalez et al., 2002). Other studies
101 showed that the rs1024611 G allele is associated with increased CCL2 levels in the plasma,
102 urine, and cerebrospinal fluid in health and disease, and in tissues such as liver and skin (Cho
103 et al., 2004; Fenoglio et al., 2004; Joven et al., 2006; Letendre et al., 2004; McDermott et al.,
104 2005). The rs1024611 polymorphism has been associated with several diseases, including
105 myocardial infarction (McDermott et al., 2005), carotid atherosclerosis (Alonso-Villaverde et
106 al., 2004), pulmonary tuberculosis (Flores-Villanueva et al., 2005), severe acute pancreatitis
107 (Cavestro et al., 2010), lupus nephritis (Tucci et al., 2004), asthma susceptibility and severity
108 (Szalai et al., 2001), Crohn's disease (CD) (Palmieri et al., 2010), Alzheimer's disease
109 (Fenoglio et al., 2004), and infections by Japanese Encephalitis virus (Chowdhury and Khan,

110 2017) and SARS-CoV-1 (Tu et al., 2015). Notably, rs3091315, a GWAS risk variant for CD
111 (Franke et al., 2010) and inflammatory bowel disease (IBD) (Liu et al., 2015) is in a strong
112 linkage disequilibrium (LD) with both rs1024611 (D′=1.0, r^2=0.98) and rs13900 (D′=1.0,
113 r^2=0.98) in the CEU population. Given the importance of disease associations with rs1024611,
114 significant efforts have been made by other groups and us to understand the molecular basis
115 of this differential CCL2 expression associated with this polymorphism (Gonzalez et al., 2002;
116 Mummidi, Bonello and Ahuja, 2009; Page et al., 2011; Pham et al., 2012; Wright et al., 2008).
117 However, these studies did not provide a mechanistic link between the rs1024611
118 polymorphism and CCL2 expression, giving rise to the possibility that SNPs in strong LD with
119 rs1024611 could be mediating these effects.
120
121 To identify potential functional SNPs that could explain the variability in CCL2 expression, we
122 developed an extensive LD map of the *CCL2* genomic locus and reported that a SNP
123 designated as the rs13900 (NM_002982.4:c.*65=) in the *CCL2* 3' UTR is in perfect LD with
124 rs1024611 and can serve as its proxy (Pham et al., 2012). We and others have demonstrated
125 AEI in *CCL2* using rs13900 as a marker with the T allele showing a higher expression level
126 relative to C allele (Johnson et al., 2008; Pham et al., 2012). In this study, we show that the
127 differential binding of Human Antigen R (HuR), an RBP previously implicated in CCL2
128 expression, leads to altered stability and translatability of *CCL2* transcripts providing a
129 mechanistic explanation for increased CCL2 expression in individuals with the rs1024611G-
130 rs13900T haplotype and inter-individual differences in disease susceptibility associated with
131 this haplotype.
132

133 ## Results

134 ### Individuals heterozygous for rs13900 show AEI of *CCL2*

135 We and others have previously reported a perfect linkage disequilibrium between rs1024611
136 in the *CCL2* cis-regulatory region and rs13900 in its 3′ UTR and that rs13900 can serve as a

137 proxy for the disease-associated rs1024611 (Hubal et al., 2010; Intemann et al., 2011;
138 Kasztelewicz et al., 2017; Pham et al., 2012). We further showed that *CCL2* exhibits allelic
139 expression imbalance (AEI) in heterozygous individuals, with the rs13900 T allele (alternative
140 allele) having a higher expression than the rs13900 C allele (reference allele) (Figure 1A). For
141 this study, we recruited 47 healthy unrelated individuals (18–35-year-old) who were screened
142 for rs13900 (Figure S1). Supplementary Table 1 shows the genotype and allele frequencies
143 for rs13900 polymorphism in these recruited individuals. We found that the rs13900 C allele
144 was at a higher frequency than the rs13900 T allele and the genotype frequencies were in line
145 with Hardy-Weinberg equilibrium ($P \geq 0.05$).. We reconfirmed that *CCL2* exhibits AEI using
146 data from heterozygous individuals. For this we used total RNA obtained from LPS treated
147 PBMC as described previously (Pham et al., 2012). LPS induced *CCL2* expression in PBMCs
148 as confirmed by qRT-PCR, with about a 4.3-fold increase at 1 h, 6.09-fold increase at 3 h, and
149 1.94-fold increase at 6 h (Figure S2). We used the 3 hour stimulation in the subsequent
150 experiments as the peak *CCL2* expression was detected at this time point following LPS
151 stimulation. AEI was measured by quantifying the relative amount of the two alleles i.e.,
152 alternative allele (T) to reference allele (C), measured from the chromatogram after
153 normalization of peak intensity using PeakPeaker v.2.0 (Figure 1B and 1C)**.** This strategy
154 ensures a direct comparison between the amount of *CCL2* mRNA that is transcribed from
155 each allele or haplotype and that each allele is equally subjected to the effects of any external
156 factors. gDNA was utilized as a control. The boxplot illustrates a notable difference in the
157 detected levels of the C and T allele in the gDNA and cDNA with a higher expression of T
158 allele relative to C allele ($P < 0.005$) (Figure 1D).
159

160 ***CCL2* mRNA transcripts bearing rs13900 C and T alleles have different stability**

161 Previous studies have shown that *CCL2* mRNA is subjected to post-transcriptional regulation
162 through modulation of mRNA stability (Hao and Baltimore, 2009). Here, we determined
163 whether the rs13900 modulates mRNA stability which may in part explain AEI. We used
164 purified monocytes from four heterozygous individuals that were left untreated or stimulated

165 with LPS for 3 h. Cells were either harvested after 3 h of LPS stimulation (considered as t=0)
166 or cultured in the presence or absence of the transcriptional inhibitor actinomycin D for an
167 additional 1, 2, or 4 h. Total RNA was isolated at each time point to assess *CCL2* transcript,
168 calculated as fold induction over unstimulated cells. *CCL2* mRNA levels showed a strong
169 upregulation following LPS stimulation ($P < 0.05$) (Figure 2A). Actinomycin D treatment
170 revealed the kinetics of *CCL2* transcript degradation by determining the mRNA half-life, which
171 represents the time (expressed in hours) at which mRNA expression is 50% of the initial level
172 (Figure 2B**;** $t_{1/2}$=Ln (0.5)/slope). For *CCL2*, $t_{1/2}$=1.763 h and is in line with previously published
173 studies that *CCL2* mRNA stability is modulated following inflammatory and cytokine stimuli
174 (Hao and Baltimore, 2009; Zhai et al., 2008).
175 To rule out the confounding effects of preexisting mRNA, the relative stability of rs13900 C-
176 and T-allele bearing transcripts in heterozygous individuals were evaluated using nascent
177 RNA. Using nascent RNA allows accurate determination of mRNA decay by eliminating the
178 effects of preexisting mRNA. Briefly, monocytes were stimulated with LPS in presence of 5-
179 ethynyl uridine (EU) for 3 hours. Cells were then washed and further incubated with or without
180 Actinomycin D for up to 4 hours. Following Actinomycin D treatment, the nascent RNA was
181 captured after 0, 1, 2 or 4 h using click reaction technique. The click reaction adds a biotin
182 handle to nascent RNA which is then captured by streptavidin beads. cDNA was synthesized
183 from the captured nascent RNA, PCR-amplified and expression of the individual alleles was
184 assessed as described above. While the allelic ratio in the no Act-D samples was ~1.6 in
185 accordance with our initial observation, the allelic ratio was further increased in presence of
186 Act-D. This suggests that post transcriptional mechanisms such as RNA stability may be
187 playing a role in rs13900 mediated CCL2 AEI.
188

189 **Bioinformatic analyses of rs13900**

190 While previous experimental studies showed that *CCL2* 3′ UTR binds HuR, it is not known
191 whether rs13900 disrupts or alters HuR binding (Fan et al., 2011; Lebedeva et al., 2011).

192 Therefore, we analyzed the rs13900 flanking region using various bioinformatic software to
193 mine existing whole genome datasets (e.g., PAR-CLIP datasets) and to predict any mRNA
194 structural changes and altered RBP motifs (Supplementary Table 2). We used AURA to
195 examine the colocalization between rs13900 and HuR (Figure 3A). As genetic variants can
196 also alter mRNA secondary structure, we used ViennaRNA package to assessed changes in
197 the *CCL2* secondary structure due to rs13900. As shown in Figure 3B, rs13900 T allele could
198 potentially alter the *CCL2* transcript secondary structure (red arrow). Further bioinformatic
199 analysis was performed using POSTAR3 suite which incorporates HOMER (Heinz et al.,
200 2010) for motif analysis and RNA context (Kazan et al., 2010) that identifies not only known
201 but also predicts relative binding and structural preferences of RBPs. HOMER motif analysis
202 (Heinz et al., 2010) identified a HuR binding motif in the region flanking the rs13900 (Fig. 3C).
203 Figure 3D shows the relative structural preference of HuR to different structural contexts
204 identified by RNAcontext, where the letters P, L, U, M indicate that the nucleotide is paired
205 (P), in a hairpin loop (L), in an unstructured (or external) region (U), or Miscellaneous (M). The
206 M category includes various unpaired contexts such as nucleotide localizing to a bulge,
207 internal loop or multiloop. The rs13900 C allele to rs13900 T allele transition is predicted to
208 form a stem (Figure 3B) which is predicted to increase HuR binding. The score of 1e was
209 obtained using RBP-Var, a bioinformatics tool that scores variants involved in post-
210 transcriptional interaction and regulation (Mao et al., 2016). Here, the annotation system rates
211 the functional confidence of variants from category 1 to 6. While Category 1 is the most
212 significant category and includes variants that are known to be expression quantitative trait
213 loci (eQTLs), likely affecting RBP binding site, RNA secondary structure and expression,
214 category 6 is assigned to minimal possibility to affect RBP binding. Additionally, subcategories
215 provide further annotation ranging from the most informational variants (a) to the least
216 informational variant (e). Reported 1e denotes that the variant has a motif for RBP binding.
217 Although the employed scoring system is hierarchical from 1a to 1e, with decreasing
218 confidence in the variant's function. However, all the variants in the category 1 are considered

219 potentially functional to some degree. Taken together, our bioinformatic analyses suggested
220 that the rs13900 allele could potentially alter the binding of HuR to *CCL2* 3′ UTR.

221

222 **Differential binding of HuR to rs13900 C and T alleles *in vitro***

223 To experimentally verify our bioinformatic findings on rs13900, we utilized RNA electrophoretic
224 mobility shift assay (REMSA) to determine whether the region of CCL2 3′ UTR that flanks
225 rs13900 binds *in vitro* to HuR and if there are allelic differences in binding. Purified labeled
226 single-stranded oligoribonucleotides corresponding to either rs13900 C or rs13900 T alleles
227 were incubated with 10 µg of whole cell extracts. We tested whether the bound complexes
228 contained HuR by performing antibody mediated supershift assays. As shown in Figure 4A
229 and 4B, a predominant shift was observed for the oligoribonucleotide corresponding to
230 rs13900 T allele (lane 8). Notably, there was an approximately 7-fold difference ($P < 0.005$) in
231 oligoribonucleotide/HuR/antibody complexes generated with oligoribonucleotide
232 corresponding to rs13900 T allele which compared to those generated with rs13900 C allele
233 (lane 4). The specificity of the complex formation was confirmed by using a non-specific
234 antibody (Figure 4A**,** lanes 3 & 7). To rule out the possibility that additional RBPs are involved
235 in this complex formation, we used purified HuR protein in mobility shift assays. These studies
236 with purified protein further confirmed that oligoribonucleotides corresponding to rs13900 C
237 or T alleles differentially bound HuR (Figure 4C)**.** Taken together, these studies provided
238 experimental validation that the rs13900 may influence differences in binding affinity to HuR
239 (Figure 4D).

240

241 **Differential binding of HuR to rs13900 C and T alleles *ex vivo***

242 We next tested the hypothesis that the rs13900 is associated with altered binding affinity to
243 HuR *ex vivo*. For this, we performed RNA immunoprecipitation in monocyte/macrophages
244 derived from four heterozygous individuals. Immunoprecipitations were performed using

245 cytoplasmic lysates of macrophages treated with LPS using an affinity purified HuR antibody
246 or IgG. Figure 5A shows the relative enrichment of HuR in the immunoprecipitated fraction
247 compared to the IgG control. The HuR immunoprecipitated fraction showed significant
248 enrichment ($P < 0.05$) of the region encompassing rs13900 when compared to the IgG control
249 (Figure 5B-C). *CCL2* transcript was enriched ~10-fold in the HuR immunoprecipitated fraction
250 in comparison to the IgG bound fraction (Figure 5C). Notably, transcripts corresponding to
251 rs13900 T allele were enriched relative to transcripts containing rs13900 C allele ($P < 0.05$)
252 in the anti-HuR RIP complexes (Figure 5D).
253
254 **rs13900 T allele confers increased mRNA stability in reporter assays**
255 As HuR is implicated in mRNA stability of many mRNA transcripts including *CCL2*, we tested
256 the hypothesis that *CCL2* 3′ UTR influences its stability and that rs13900 modulates this effect.
257 We constructed reporter plasmids that harbor the *CCL2* 3′ UTR containing either rs13900 C
258 or rs13900 T allele (Figure 6A) and nucleofected them into HEK293 cells as described in
259 Materials and Methods. Luciferase activity was measured after 24 h post-transfection (Figure
260 6B). Our results indicated that the presence of *CCL2* 3′ UTR significantly ($P < 0.05$) reduced
261 the luciferase activity. However, cells transfected with plasmids bearing the rs13900 T allele
262 showed higher luciferase activity when compared with cells transfected with plasmids bearing
263 the rs13900 C allele, suggesting that the presence of rs13900 T allele conferred increased
264 stability to the transcript ($P<0.05$). We next analyzed the influence of HuR overexpression in
265 reporter vectors containing *CCL2* 3′ UTR with either rs13900 C or T alleles. Overexpression
266 of HuR led to a significant increase in luciferase activity of the reporter vector bearing rs13900
267 T allele ($P < 0.05$), However, HuR overexpression had no significant effect on the luciferase
268 activity of the reporter vector bearing the rs13900 C allele (Figure 6C). Conversely, we
269 examined the effect of HuR on the expression of the reporter assay by co-transfection of HuR
270 siRNA and luciferase reporter constructs. While HuR knockdown had no effect on luciferase
271 activity of the reporter construct bearing rs13900 C allele, it caused a significant reduction in

272 luciferase activity of construct bearing the rs13900 T allele ($P < 0.05$) (Figure 6D). The
273 overexpression and knockdown of the HuR in the nucleofected cells was confirmed using
274 Western blots (Figure S3).
275
276 **Role of HuR-rs13900 interactions in *CCL2* mRNA translatability**
277 The differential interactions with HuR by rs13900 C and rs13900 T alleles could potentially
278 alter *CCL2* mRNA translatability as HuR could increase mRNA translation (Schultz et al.,
279 2020). Therefore, we assessed the relative allelic enrichment in the monosomal and polysomal
280 fractions obtained from MDMs from two individuals exhibiting AEI. Translationally active and
281 inactive pools of RNA were fractionated by isolating the monosomal and polysomal fractions
282 from MDMs on sucrose gradients after the cells were treated with cycloheximide to block
283 translation. The distribution of *CCL2* mRNA in macrophages cultured in presence or absence
284 of LPS for 3 h is depicted in Figure S4. As previously reported by others, LPS treatment
285 resulted in a distinct shift of the mRNAs from monosomal fraction to the polysomal fraction
286 (Schott et al., 2014). Consistent with this prior report, 60.4% of the *CCL2* mRNA was
287 associated with polysomal fraction following stimulation of cells with LPS. We assessed the
288 differences in allelic enrichment in cytosolic, monosomal, and polysomic fractions and found
289 that the polysomal fractions showed the enrichment of the rs13900 T allele (Supplementary
290 Table 3). However, this differential loading of rs13900 T allele was noted for one donor in
291 cytosolic and monosomal fractions as well.
292 To further address this question, we used a reporter-based system to assess the effect of
293 rs13900 C and T alleles on the translatability as previously reported (Zhang et al., 2017). To
294 measure translatability, luciferase mRNA and protein were measured simultaneously, and
295 translatability was calculated as luciferase activity normalized by the luciferase mRNA levels
296 after adjusting for protein and 18S rRNA (Figure 7A-C). Our results suggest that the rs13900
297 may alter the mRNA translatability in addition to the transcript stability.
298
299

300 **Differential effect of HuR over-expression on the *CCL2* rs13900 T allele**

301 Our *in vitro* and *ex vivo* data indicate that HuR positively regulates *CCL2* transcript stability by
302 increased binding to the T allele. To determine a direct functional relationship between HuR
303 and *CCL2* AEI, we used a lentiviral overexpression system. We either transduced HuR specific
304 (pCMV6-HuR) or non-specific control shRNAs (CMV-null) into the monocytes obtained from
305 donors who were either homozygous for rs13900 C or T allele. Ready to use GFP-tagged
306 pCMV6-HuR or CMV-null lentiviral particles were transduced into macrophages in the
307 presence of polybrene at an MOI of 1. Cells were processed 72 h following virus addition for
308 the analysis of HuR and *CCL2* mRNA expression. Using this lentiviral system, both high
309 transduction efficiency (90%) and high expression levels were achieved in primary human
310 macrophages (Figure S5). Compared with CMV-Null particles, substantial overexpression of
311 HuR was noted with pCMV6-HuR lentiviral particles (Figure 8A). HuR overexpression was
312 associated with a higher expression of *CCL2* mRNA in persons homozygous for T allele
313 relative to those who were homozygous for C allele (Figure 8B).

314

315 ## Discussion

316 Genome-wide association studies (GWASs) have led to the discovery of numerous disease
317 susceptibility genetic variants/genes and biological pathways involved in specific diseases,
318 including many with immunological etiologies (Buniello et al., 2019; Manolio, 2010; Visscher
319 et al., 2017). Most of the disease-associated genetic variants identified are present in the non-
320 coding regions of the genome (Maurano et al., 2012; Zhang and Lupski, 2015; Zou et al.,
321 2019). However, characterizing the functional consequence of these genetic variants in the
322 regulatory regions remains a significant challenge to date. About 3.7% of the non-coding
323 variants localize to the untranslated regions (Steri et al., 2018), suggesting post-transcriptional
324 mechanisms such as mRNA stability and translatability could determine disease susceptibility
325 (Maurano et al., 2012).

326

327 The *CCL2* locus exemplifies the difficulty in dissecting the functional consequences of cis-
328 regulatory and non-coding genetic variants. Our analysis of regulatory elements in an ~20 kb
329 region upstream of the human *CCL2* coding region identified highly conserved enhancers and
330 other regulatory elements in the *CCL2* locus (Bonello et al., 2011). We identified SNPs with
331 strong LD in this "super-enhancer" and determined their impact on transcriptional activity,
332 which was minimal (Pham et al., 2012). For example, we tested the role of rs7210316 and
333 rs9889296, which had an $r^2 > 0.9$ with rs1024611 in CEU population and were located ~6.3
334 kb and ~9.2 kb upstream of it (Pham et al., 2012). The genetic regions that encompass and
335 flank these two SNPs either had no or minimal transcriptional activity and lacked the epigenetic
336 markers that have been traditionally associated with gene activation. Additionally, conflicting
337 context-dependent results have been obtained for the transcriptional activities associated with
338 reporter vectors containing rs1024611 A and G alleles, which may have been due to the use
339 of different lengths of the *CCL2* cis-regulatory regions employed in the transcriptional assays.
340 To avoid such context-dependent confounding, we used chromatin annotation, a powerful
341 approach to identify functional SNPs, to generate reporter constructs that span a 6 kb cis-
342 regulatory region (Pham et al., 2012). This approach allowed us to directly compare the roles
343 of four correlated SNPs (rs1860190, rs2857654, rs1024611, and rs2857656) on *CCL2*
344 transcriptional activity. We found no significant differences in transcription strength between
345 these two constructs when transfected into primary human astrocytes (Pham et al., 2012).
346 Furthermore, to understand the basis for increased CCL2 expression associated with the
347 rs1024611 G allele, we and others have demonstrated that several transcription factors bind
348 differentially to *CCL2* polymorphisms, including IRF-1, PARP-1, STAT-1, Prep1/Pbx
349 complexes (Gonzalez et al., 2002; Mummidi, Bonello and Ahuja, 2009; Page et al., 2011;
350 Wright et al., 2008). However, these previous studies could not unequivocally demonstrate
351 the mechanistic link between differential binding of transcription factors and transcriptional
352 activity and the physiological relevance of implicated transcription factors in CCL2 expression.
353 Our comprehensive studies outlined here demonstrate that rs13900 T allele differentially binds
354 to the RBP HuR, which could alter CCL2 mRNA stability and gene expression. Furthermore,

355 we provide multiple lines of functional evidence for rs13900/HuR role in *CCL2* AEI, including
356 reporter vector assays and HuR overexpression and depletion experiments.
357
358 Our previous finding that rs13900 is in perfect LD with rs1024611 has allowed us to exploit
359 the powerful AEI technique and mechanistically link the *CCL2* rs1024611G-rs13900T
360 haplotype to increased expression (Pham et al., 2012). These findings, together with previous
361 knowledge that *CCL2* is subjected to post-transcriptional regulation (Hao and Baltimore, 2009)
362 and regulated by RBP (Fan et al., 2011), raised the possibility that rs13900 could be functional
363 and impact mRNA stability and translatability. In this study, we determined the half-life of *CCL2*
364 to be 1.76 h, reinforcing the fact that post-transcriptional regulation is a key feature of *CCL2*
365 expression (Fig.2B). Since transcription and RNA degradation are tightly linked, and
366 transcriptional inhibition may lead to mRNA decay, we assessed the allelic differences in
367 expression in nascent RNA obtained from heterozygous individuals. We found that the *CCL2*
368 transcripts with rs13900 T allele have increased stability relative to those with rs13900 C allele
369 (Figure 2C). In addition, both rs1024611 and rs13900 have suggestive associations with *CCL2*
370 expression in *cis*-expression quantitative trait loci (eQTL) analyses. For example, rs1024611
371 and rs13900 are associated with CCL2 expression in MDM infected with *Listeria*
372 *monocytogenes* (Nedelec et al., 2016) (−log10(p) = 3.19; Effect size = 0.29±0.084) (Kwong et
373 al., 2021). Remarkably, rs13900 is also identified as a cis-splicing quantitative trait locus (cis-
374 sQTL) for *CCL2* in both untreated and treated monocytes (Alasoo et al., 2018; Kwong et al.,
375 2021; Quach et al., 2016). Recent evidence suggests that genetic variation influencing RNA
376 splicing could play an important role in determining complex phenotypic traits (Li et al., 2016).
377 While rs13900 serves as an sQTL for several *CCL2* transcripts variants, we provide an
378 illustrative example here. rs13900 showed significant associations with the canonical *CCL2*
379 transcript, ENST00000225831 in LPS treated monocytes (−log10(p) = 9.88; Effect size =
380 0.57±0.084) and with a CCL2 transcript ENST00000580907 (−log10(p) = 9.88; Effect size =
381 −0.57±0.084) that encodes a truncated CCL2 protein (Kwong et al., 2021). While the
382 importance of these associations needs more in-depth studies, our observation that *CCL2*

383 transcripts with rs13900 T allele have a slower degradation could explain the increased CCL2
384 expression in individuals with rs1024611G-rs13900 haplotype as modest changes in mRNA
385 stability can lead to significant effects on mRNA and protein abundance.
386
387 Post-transcriptional gene expression is regulated through interactions between the *cis*-
388 elements in mRNAs and their cognate RBPs (Wu and Brewer, 2012). Studies indicate
389 presence of post-transcriptional operons or regulons – unique subsets of RNAs that associate
390 with RBPs, which coordinate their localization, translation, and degradation. Our
391 bioinformatics analysis and experimental data confirm HuR binds to the region spanning the
392 rs13900. iClip data from HeLa cells (Wang et al., 2010), suggested that the RBPs TIAL1 (T
393 cell intracellular antigen-1 like protein) and U2AF65 (U2 snRNP auxiliary factor large subunit)
394 could also bind to this region of the *CCL2* transcript (Mao et al., 2016). TIAL1 has been
395 proposed to act as a cellular sensor and has been associated with a transcriptome associated
396 with control of inflammation, cell-cell signaling, immune-suppression, angiogenesis,
397 metabolism and cell proliferation (Reyes, Alcalde and Izquierdo, 2009). The role of TIAL1 in
398 *CCL2* expression is not known and additional studies are needed to determine if its binding
399 contributes to *CCL2* AEI. U2AF65 is a widely expressed splicing factor that associates with
400 RNA polymerase II to bind upstream 3′ splice sites to facilitate splice site pairing in higher
401 eukaryotes (Hollander et al., 2016). In addition, a change in RNA structure due to a SNP could
402 indirectly alter accessibility of additional regions to RBPs and further studies are required to
403 determine any such changes (Shatoff and Bundschuh, 2020).
404
405 The Hu family contains 4 members, of which HuR is ubiquitously distributed. HuR consists of
406 three RNA recognition motifs (RRMs) that are highly conserved and canonical in nature (Ripin
407 et al., 2019). In absence of RNA the three RRMs are flexibly linked but upon RNA binding they
408 transition to a more compact arrangement. Mutational analysis revealed that HuR function is
409 inseparably linked to RRM3 dimerization and RNA binding. Dimerization enables recognition
410 of tandem AREs by dimeric HuR (Pabis et al., 2019) and explains how this versatile protein

411 family can regulate numerous targets found in pre-mRNAs, mature mRNAs, miRNAs and long
412 noncoding RNAs. HuR shuttles between the nucleus and cytoplasm and is likely involved in
413 the transport and stabilization of mRNA. HuR action is antagonized by RNA destabilizing
414 proteins such as TTP (tristetraprolin) and AUF (ARE/poly(U)-binding/degradation factor 1)
415 (Wu and Brewer, 2012). The role of HuR in chemokine gene regulation has been extensively
416 studied in human airway epithelium cells (Fan et al., 2011), they identified that *CCL2* is one
417 of the top targets for HuR and demonstrated that HuR associated with *CCL2* 3′ UTR *in vitro*
418 and *CCL2* expression could be modulated by changes in HuR levels using overexpression
419 and RNAi-based experiments. Also, HuR levels influenced *CCL2* mRNA decay. In a mouse
420 model of alcoholic liver disease, HuR was found to play a key role in NOX4 mediated increase
421 in *CCL2* mRNA stability (Sasaki et al., 2017). Notably, HuR has also been implicated in mRNA
422 stability of CX3CL1 (Matsumiya et al., 2010) and IL-8 (Choi et al., 2009) among others.
423 Another study showed that CCL2 itself can induce nuclear to cytoplasmic translocation of HuR
424 and stabilize vascular endothelial growth factor-A (*VEGFA*) mRNA in $CD14^{+}CD16^{low}$
425 inflammatory monocytes, thus raising the possibility that CCL2 may stabilize its own message
426 in an autocrine fashion (Morrison et al., 2014). These studies further bolster a role for HuR in
427 *CCL2* expression and support our finding that differential binding to HuR alters its expression
428 level.
429
430 While there are several examples of genetic variants that influence mRNA stability (Akdeli et
431 al., 2014; Duan et al., 2013; Vilmundarson et al., 2021; Wang, Pitarque and Ingelman-
432 Sundberg, 2006), very few studies have examined the role of RBPs such as HuR in
433 differentially influencing gene expression levels in humans (Steri et al., 2018). A notable
434 exception is the report showing that RBP AUF1 regulates the allele-specific stability of
435 thymidylate synthase (Pullmann et al., 2006). Another study showed that a type 2 diabetes
436 associated polymorphism in the 3′ UTR of *PPP1R3* alters distance between two ARE motifs
437 and results in differential binding of protein complexes and may be associated with altered
438 mRNA stability (Xia, Bogardus and Prochazka, 1999). Vilmundarson et al. demonstrated that

439 HuR differentially modulates *IRF2BP2* translation through a 3′ UTR polymorphism that is
440 associated with increased coronary artery calcification (Vilmundarson et al., 2021). Our
441 exploratory studies did not resolve whether the rs13900 allelic variation leads to differences
442 in polysomal loading and additional studies are required to address this issue. Another
443 important mechanism by which disease associated genetic variants in the UTRs could
444 influence mRNA stability and translatability is by disrupting or creating microRNA binding sites
445 (Huang et al., 2019). We examined the region flanking the rs13900 and found that there are
446 several predicted binding sites for miRNAs. Among these, several miRNAs have minimum
447 free energy ≤ –25 kcal/mol suggesting that they can potentially play a role in *CCL2* expression
448 and will be investigated in future studies. Of note, a recent study showed that RBPs may play
449 an important role in miRNA mediated gene regulation (Kim et al., 2021).
450
451 RBPs regulate the protein expression from a given mRNA by modulation of its half-life,
452 subcellular localization, and ribosomal recruitment (Glisovic et al., 2008). However**,** mRNA
453 abundance and stability are not always predictive of protein synthesis: relative mRNA
454 abundance/stability and translation levels of a given gene can vary significantly and
455 determined by an assortment of post-transcriptional events (Liu, Beyer and Aebersold, 2016).
456 Our previous findings and results from the present study suggest that there is a close
457 association between *CCL2* rs1024611-rs13900 haplotype, mRNA, and protein expression.
458 Nevertheless, we cannot completely rule out the contribution of transcription-based
459 mechanisms to the allelic expression imbalance at the *CCL2* locus. Previous studies have
460 suggested that there is a high level of conservation for interactions between RBPs and their
461 target molecules and that RNA-mediated gene regulation is less evolvable than transcriptional
462 regulation (Payne, Khalid and Wagner, 2018). Thus, it is remarkable that the rs13900 alters
463 HuR binding and impacts both transcript stability and translatability. Our bioinformatic analysis
464 shows that rs13900 could potentially lead to dramatic changes in the secondary structure of
465 *CCL2* mRNA (Fig. 3B). A recent study using bioinformatic analyses has shown that SNPs may
466 affect RNA-protein interactions from outside binding motifs through altered RNA secondary

467 structure (Shatoff and Bundschuh, 2020). We cannot rule out the possibility that HuR may
468 differentially bind to other regions of *CCL2* transcript due to changes in secondary structure
469 and therefore needs to be examined in future studies.
470 Given our findings that rs13900 modulates HuR binding and thereby influences *CCL2*
471 expression, targeting HuR-ARE interactions could offer a promising therapeutic avenue for
472 conditions involving heightened monocyte/macrophage recruitment, such as inflammatory,
473 cardiovascular, and neoplastic diseases. Indeed, existing small-molecule inhibitors of HuR
474 (e.g., MS-444, KH-3, and CMLD-2) (Chaudhary et al., 2023; Fattahi et al., 2022; Lang et al.,
475 2017; Liu et al., 2020; Wang et al., 2019; Wei et al., 2024) highlight the feasibility of disrupting
476 HuR function in vivo, suggesting that co-targeting HuR and the rs13900 may represent a
477 novel precision-based strategy for monocyte/macrophage- driven disorders.

478

479 Both rs1024611 and rs13900 are in high LD with rs3091315, which is detected in the GWA
480 studies of CD and IBD (de Lange et al., 2017; Franke et al., 2010; Kenny et al., 2012; Liu et
481 al., 2015; Palmieri et al., 2010). rs3091315 is classified as an upstream risk variant and is
482 located in the intergenic region between *CCL2* and *CCL7*. The GWA risk allele for CD is
483 rs3091315-A which is correlated with rs1024611(A) and rs13900(C) alleles. While the
484 biological role of *CCL2* in CD and IBD are well recognized (Darkoh et al., 2014; Maharshak et
485 al., 2010; Martin et al., 2019), the results from genetic association studies are not consistent
486 and the disease outcomes could potentially differ by population studied (Chen et al., 2016).

487

488 In conclusion, our study shows that the disease associations mediated by the *CCL2*
489 rs1024611-rs13900 haplotype may be due to altered mRNA stability mediated through
490 differential binding of an RBP. Given the importance of mRNA stability in immune homeostasis
491 such mechanisms could play a critical role in inter-individual differences in disease
492 pathogenesis.

493

494 **Materials and Methods**

495 **Recruitment of study participants, primary cell culture, and genotyping**

496 All research involving human subjects were approved by the Institutional Review Boards
497 (IRBs) of the University of Texas Health San Antonio, San Antonio, Texas and University of
498 Texas Rio Grande Valley, Edinburg, Texas and Texas A&M University- San Antonio. Written,
499 informed consent from each individual for participation in our study was obtained following the
500 IRB approval. A total of 47 unrelated individuals were recruited into the study. Data and
501 samples from the study participants were obtained at the First Outpatient Research Unit
502 (FORU), UT Health San Antonio, San Antonio, Texas. The rs13900 polymorphism was
503 detected by TaqMan predesigned SNP genotyping assay (Applied Biosystems, CA, USA, Cat.
504 No. 4351379). Briefly, genomic DNA samples were obtained from peripheral blood of healthy
505 study participants using QIAamp DNA Blood Mini Kits (QIAGEN, Cat. No 51104) in
506 accordance with the manufacturer's protocol, checked for quality and concentration, and
507 stored at −80ºC until used. Genotyping of rs13900 was performed on 10 ng of genomic DNA
508 using TaqMan genotyping Master mix in a 10 µL reaction volume. PCR was performed on the
509 Quantstudio 12K Flex (Applied Biosystems) in 384-well plates. The temperature cycling
510 conditions consisted of an initial enzyme heat-activation step of 10 min at 95ºC and 40 cycles
511 of a 3-step amplification profile of 20 sec at 95ºC for denaturation, 1 min at 60ºC for annealing,
512 and 30 sec for 72ºC for extension. QS12K software (Applied Biosystems, CA, USA). was used
513 to score the alleles. Whole blood samples were collected from study participants who were
514 either homozygous (either C/C or T/T) or heterozygous (C/T) for rs13900 at the initial
515 screening for the genotype status, followed by recalling selected individuals for detailed
516 studies. Peripheral blood mononuclear cells (PBMC) were isolated by a Ficoll density gradient
517 centrifugation. Total genomic DNA and RNA were isolated from $0.5x10^6$ PBMC following
518 stimulation with 1 µg/mL LPS (Millipore Sigma, Cat No. L2630) for 3 h as described previously
519 (Pham et al., 2012; Sharif et al., 2007). CD14+ monocytes were purified using EasySep
520 Human Monocytes Isolation Kit (negative selection kit; Stem cell Technologies, Cat No.
521 19359) according to manufacturer's instructions. Monocytes were treated with 50 ng/ mL M-

522 CSF (Peprotech, Cat No. 300-25) for 72 h to induce macrophage differentiation, and flow
523 cytometric measurement of surface markers CD64 (BD-Pharmigen, Cat No. 555522), CD206
524 (BD-Pharmigen, Cat No.564060), and CD44 (BD-Pharmigen, Cat No. 555479) was used to
525 confirm the differentiation (Figure. S6).
526
527 **Real-time quantitative PCR (RT-qPCR) assays**
528 Total RNA was isolated using the RNeasy plus mini kit (Qiagen, Cat No. 74134) according to
529 manufacturer's instructions. 10 µL of total RNA sample (500 ng) was converted to cDNA using
530 MultiScribe Reverse Transcriptase (Applied Biosystems, Cat No. 4311235) with random
531 primers. Real-time quantitative PCR was performed using TaqMan gene expression assays
532 (ThermoFisher Scientific, Cat No. 4331182). Relative expression levels were calculated by
533 applying the $2^{-\Delta\Delta Ct}$ method using 18S rRNA as a reference.
534
535 **Capture of nascent RNA**
536 Newly synthesized RNA was isolated using the Click-It Nascent RNA Capture Kit (Invitrogen,
537 Cat No: C10365) following the manufacturer's protocol. Peripheral blood mononuclear cells
538 (PBMCs) or monocyte-derived macrophages (MDMs) obtained from heterozygous individuals
539 were stimulated with 1 µg/mL lipopolysaccharide (LPS) for 3 hours, followed by a 3-hour pulse
540 with 0.2 mM 5-ethynyl uridine(Jao and Salic, 2008; Paulsen et al., 2013). After the pulse, the
541 culture medium was replaced with fresh growth medium devoid of EU. To assess RNA
542 stability, cells were left untreated or were treated with actinomycin-D (5 µg/mL) and samples
543 were collected at 0, 1, 2, and 4 h post-treatment. The EU RNA was subjected to a click reaction
544 that adds a biotin handle which was then captured by streptavidin beads. The captured RNA
545 was used for cDNA synthesis (Superscript Vilo kit, Cat No: 11754250), PCR amplification, and
546 allelic quantification.
547
548

549 **AEI assessment of *CCL2***

550 Total RNA and genomic DNA were isolated from primary immune cells (PBMC and
551 macrophages) after they were treated with LPS for 3 h. Total RNA was reverse transcribed as
552 described above. The region encompassing rs13900 was amplified by PCR in a 50 μL
553 reaction mixture containing 2 μL of cDNA or genomic DNA, 25 μL AmpliTaq Gold 360 Master
554 Mix (ThermoFisher Scientific, Cat No: 4398881) and 10 μM each of the forward and reverse
555 primers. The nucleotide sequence of the forward primer and reverse primers were 5′-
556 ACCTGGACAAGCAAACCCAA-3′ and 5′- ACCCTCAAAACATCCCAGGG-3′. The following
557 temperature conditions were used: initial denaturation at 95ºC for 10 min followed by 40 cycles
558 of denaturation at 95ºC for 30 s, annealing at 53.6ºC for 30 s, extension at 72ºC for 30 s, and
559 final extension at 72ºC for 7 min. The amplicons were purified with The GeneJET PCR
560 Purification Kit (ThermoFisher Scientific, Cat No: K0701) and were subjected to Sanger
561 sequencing (Macrogen,USA) using the sequencing primer 5′-
562 GCAAACCCAAACTCCGAAGAC-3′. The degree of AEI for *CCL2* was expressed as a ratio of
563 reference allele (REF; major) to alternative allele (ALT; minor). PeakPicker,v.2.0 was used
564 with default settings to quantify the relative amount of the two alleles from the chromatogram
565 after peak intensity normalization (Ge et al., 2005).

566

567 **Bioinformatic analyses**

568 The ex vivo binding of RBPs to region flanking rs13900 and *CCL2* 3′ UTR was examined using
569 Atlas of UTR Regulatory Activity (AURA) (Dassi et al., 2014). The resources included in
570 POSTAR3 were used to interrogate the RNA binding motifs that overlap the rs13900 (Zhao et
571 al., 2022). RBP-var2 was used to explore the potential functional consequences (Mao et al.,
572 2016), and the ViennaRNA package (Lorenz et al., 2011) was used to predict changes in
573 *CCL2* secondary structure due to rs13900.

574

575

576 **RNA electrophoretic mobility shift assay (REMSA)**

577 Oligoribonucleotides spanning the rs13900 C or rs13900 T alleles (IDT) labeled with infrared
578 dyes were used to determine the differential binding of HuR. The sequences of the
579 oligoribonucleotide with rs13900 C allele is
580 rCrUrUrUrCrCrCrCrArGrArCrArCrCr**C**rUrGrUrUrUrUrArUrUrU and oligoribonucleotide with
581 rs13900 T allele is rCrUrUrUrCrCrCrCrArGrArCrArCrCr**U**rUrGrUrUrUrUrArUrUrU. The
582 oligoribonucleotides were incubated with either 10 µg HuR overexpressing HeLa cell whole
583 cell extracts or 25-200 µM ELAVL1 human recombinant protein (Origene, Cat No: TP301562)
584 in a 20 µL reaction mixture with 20 units of RNasin and 1X RNA binding buffer containing 20
585 mM HEPES (pH 7.6), 3 mM $MgCl_2$, 40 mM KCl, 5% glycerol and 2 mM dithiothreitol, 20 µg
586 yeast tRNA. The reaction was incubated on ice for 10 min and super-shift assay was
587 performed by adding 2 µL of anti-HuR antibody (3A2, mouse monoclonal IgG antibody, Santa
588 Cruz Biotechnology, Cat No: sc-5261). After antibody addition, the complexes were incubated
589 on ice for 15 min and were resolved by electrophoresis under non-denaturing conditions in
590 5% polyacrylamide gels with 0.5 × TBE running buffer. Gels were then analyzed using Li-Cor
591 Odyssey CLX.

592

593 **RNA-binding protein immunoprecipitation**

594

595 RNA-binding protein immunoprecipitation (RIP) was carried out using an
596 immunoprecipitation kit (RIP-assay kit, MBL) following the manufacturer's instructions.
597 Briefly $2x10^6$ cells were lysed and the extract was precleared and incubated with 15 µg
598 of antibody against HuR or IgG for 3 h. RNA on the beads was purified and converted
599 to cDNA using random hexamer. cDNA was further amplified and the PCR product
600 sequenced using the following primer: GCAAACCCAAACTCCGAAGAC.

601

602

603 **Cell culture and transfection**

604 HEK-293 cell line was maintained in EMEM (ATCC) containing 10% heat-inactivated FBS,
605 penicillin (100 U/mL) and streptomycin (100mg, mL) (GIBCO). Cells were cultured at 37ºC in
606 humidified air containing 5% CO_2. For HuR overexpression and silencing studies, cells were
607 seeded in six-well plates in serum-free EMEM at a density of ~ 250,000 cells per well. The
608 cells were transfected when they reached ~ 70 to 80% confluency, using lipofectamine 3000
609 (ThermoFisher Scientific, Cat No: L3000008) according to the manufacturer's recommended
610 protocol. Briefly, lipofectamine 3000 was diluted in OptiMEM and allowed to complex with
611 either 0.5 µg of pCMV6-HuR or pCMV-Entry plasmid or 50 µM of HuR siRNA or control siRNA
612 for 15 min at room temperature. The plasmid/siRNA-lipofectamine 3000 mixture was then
613 added to the cells in a final volume of 2 mL of complete medium. After incubation for 72 h,
614 cells were harvested and used for further processing.

615

616 **Western blotting**

617 Cell lysates were prepared in chilled RIPA buffer (25 mM Tris-HCL pH 7.6, 150 mM NaCl, 1%
618 NP-40, 1% sodium deoxycholate, 0.1% SDS; Thermo Scientific, Rockford, IL) containing
619 protease inhibitor (complete Mini, EDTA-free Protease inhibitor cocktail tablets, Roche
620 Diagnostics, Cat No: 11836170001). Cells were lysed on ice for 10-15 min followed by
621 centrifugation at 12,000 × g for 15 min, and the cleared supernatant was collected and stored
622 at −20ºC. Cell lysates with equal amounts of total protein (15-20 µg) were loaded and
623 separated on a SDS polyacrylamide gel (10–15%) and were electrophoretically transferred
624 onto nitrocellulose membranes (Thermo Scientific). The membranes were blocked with non-
625 fat dry milk in TBST (50 mM Tris-HCl, pH 7.4, 150 mM NaCl, 0.2% Tween 20) and were
626 incubated overnight with anti-HuR primary antibodies (diluted 1:1000). Following incubation,
627 the membranes were washed and then further incubated with anti-mouse ß-actin for one h at
628 room temperature, followed by HRP labeled goat anti-mouse or goat anti-rabbit antibodies

629 (1:1000; Santa Cruz). Protein bands were detected using a chemiluminescence (ECL kit)
630 method (Pierce) and visualized on X-ray film (Kodak).

631

632 **Reporter assays**

633 Site-specific mutagenesis was done on *CCL2* LightSwitch 3′ UTR reporter (Active Motif) to
634 generate constructs containing rs13900 C or rs13900 T alleles. The nucleotide sequence of
635 the complete constructs was verified by Sanger sequencing (Macrogen, USA). 0.5 μg of these
636 constructs were nucleofected into HEK293 cells using 4D Nucleofector (Lonza) and luciferase
637 activity was measured 24 h post transfection using Spectramax plate reader (Molecular
638 Devices). The efficiency of the nucleofection was verified by confocal microscopy, and it was
639 greater than 90%. Given the high efficiency of the nucleofection and to avoid cross-talk with
640 co-transfected control plasmids (Farr and Roman, 1992), luciferase data across samples was
641 normalized using the protein content of the lysates using BCA protein assay. mRNA
642 translatability was assessed using methods as described previously (Zhang et al., 2017).

643

644 **Polysome profiling**

645 Human monocytes were isolated from fresh blood as described earlier (Gavrilin et al., 2009)
646 with slight modification. Briefly, peripheral blood mononuclear cells were isolated by density
647 gradient centrifugation using Histopaque, followed by immunomagnetic negative selection
648 using EasySep Human Monocyte isolation kit. A high purity level for $CD14^+$ cells was
649 consistently achieved (≥90%) through this procedure, as confirmed by flowcytometry. The
650 purified monocytes were immediately used for macrophage differentiation by treating them
651 with 50 ng/mL M-CSF (PeproTech) for 72 h and flow cytometric measurement of surface
652 markers CD64+, CD206+, CD44 was used to confirm the differentiation (Fig. S6). Cells were
653 treated with LPS or PBS for 3 h to induce *CCL2* expression. Cells were treated with 0.1 mM
654 cycloheximide, a translation inhibitor, for 3 min, harvested and washed with ice-cold PBS
655 containing 0.1 mM cycloheximide, and pelleted by centrifugation for 5 min at 500 x g. The

656 pellets were either stored at −80ºC or immediately used for cytoplasmic lysate preparation.
657 The cell pellet was resuspended in 500 µL lysis buffer containing 150 mM NaCl, 50 mM Tris-
658 HCl pH 7.5, 10 mM KCl, 10 mM $MgCl_2$, 0.2% NP-40, 2 mM dithiothreitol, 2 mM sodium
659 orthovanadate, 1 mM phenylmethylsulfonyl fluoride, and 80 units/mL RNaseOUT. After 10 min
660 incubation on ice with occasional inverting every two minutes, samples were centrifuged at
661 12,000 x g for 10 min at 4°C to pellet the nuclei and the post-nuclear supernatants. The optical
662 density at 254 nm was measured, and volumes corresponding to the same OD254 were used.
663 Post-nuclear supernatants were laid on top of a 10-50% sucrose gradient. The gradient was
664 centrifuged for 90 min at 200,000 x g. After the ultracentrifugation, ten fractions were collected
665 from top to bottom. RNA was extracted from each fraction and RT-qPCR was performed using
666 *CCL2* mRNA specific primers. For analysis, fraction one was considered as cytoplasmic
667 lysate, fractions 2-4 were considered monosomal fraction, and fractions 6-10 as polysomal
668 fraction. The percent (%) distribution for the *CCL2* mRNAs across the gradients was calculated
669 using the differences in the cycle threshold (ΔCt) values using the following formula (Nayak et
670 al., 2013):
671 % of mRNA A in each fraction = $2^{\Delta CT\ fraction\ X}$ x 100/Sum, where ΔCT fraction X = CT (fraction
672 1) − CT (fraction X)
673
674 **Lentiviral transduction of primary macrophages**
675 Cells were transfected by slightly modifying the method described by Plaisance-Bonstaff et.al
676 2019 (Plaisance-Bonstaff et al., 2019). Briefly, monocytes were purified from PBMCs obtained
677 from homozygous donors for rs13900 C or rs13900T by negative selection. Upon purification
678 cells were resuspended in 24 well plates at a seeding density of 0.5 $x10^6$ cells per well and
679 were further cultured in the medium supplemented with 50 ng/mL M-CSF (Figure. S7). After
680 24 h, ready to use GFP-tagged pCMV6-HuR or CMV-null lentiviral particles (Amsbio,
681 Cambridge, M.A) were transduced into 0.5 $x10^6$ cells in presence of polybrene (60 µg/mL) at
682 a MOI of 1. The cells were processed for HuR and *CCL2* expression 72 h after transduction
683 after stimulation with LPS for 3 h.

Statistical Analyses

All values in figures are presented as the mean ± SEM. Results were analyzed with ANOVA and posthoc contrasts with Fisher (Least Significant Difference (LSD) test or Student's t test. Statistical analyses were carried out in the Sigma Plot 12.0 software.

Acknowledgments

We thank the participants of the study for their time and support.

690 **Figure Captions**

691 **Figure.1. rs13900 heterozygous individuals exhibit AEI in *CCL2*. (A)** Schematic depicting
692 distal, proximal regulatory elements extending 3 kb on either side of *CCL2* gene and the LD
693 between regulatory polymorphism rs1024611 and the transcribed polymorphism rs13900.
694 rs1024611 is located 2578 base pairs upstream of the *CCL2* translation start site and rs13900
695 located in the *CCL2* 3′ UTR. **(B)** Allelic expression imbalance (AEI) in heterozygous donors is
696 measured as a ratio of alternative allele (ALT) to reference allele (REF) in a transcribed
697 polymorphism. **(C)** Representative chromatograms obtained following Sanger sequencing of
698 PCR products obtained from genomic DNA (gDNA) and reverse transcription-PCR of mRNA
699 (cDNA) from three individuals heterozygous for rs13900. gDNA and mRNA were obtained
700 from PBMC treated with LPS for 3 h as previously described. The allelic ratios shown were
701 determined by PeakPicker analysis. Peakpicker calculates allelic ratios by dividing the peak
702 height of the alternate allele (rs13900 T allele) by that of reference allele (rs13900 C allele).
703 The gDNA peaks were used for normalization. **(D)** Allelic ratio for cDNA and gDNA in six
704 individuals heterozygous for rs13900 after treatment with LPS for 3 h. Statistical significance
705 for the difference in the level of expression between the alleles was determined using
706 Student's *t*-test ($P < 0.003$).

707

708 **Figure 2. rs13900T confers greater stability to *CCL2* mRNA. (A)** *CCL2* mRNA expression
709 in peripheral monocytes of heterozygous individuals (n = 6) after treatment with LPS for 3 h
710 and then incubated with 5 µg Act D for indicated times. mRNA was detected by RT-PCR.
711 Results, normalized to 18S rRNA levels, are expressed as folds increase over unstimulated
712 cells (CNT). Levels shown in bar graph represent mean ± SEM of result at time 0 (*$P = 0.019$)
713 versus unstimulated cells (N = 4). **(B)** *CCL2* mRNA half-life, calculated for each condition as
714 the time (in hours) required for the transcript to decrease to 50% of its initial abundance [t 1/2
715 = ln (0.5)/slope]. **(C)** Nascent RNA was isolated from treated monocytes from three individuals
716 in the presence and absence of ActD. Allelic ratio was determined after 4 h of incubation with

717 or without ActD. Expression of rs13900 T allele was much higher in ActD-treated samples.
718 The difference between the groups were assessed by ANOVA with Fisher LSD method (*P <
719 0.05, ** P < 0.005).
720
721 **Figure 3. Bioinformatic analysis of the rs13900. (A)** Validation RBP binding sites and
722 polymorphism located on the 3′ UTR of *CCL2* transcript from the Atlas of UTR Regulatory
723 Activity and analysis of ENCODE genome-wide data sets detected specific enrichment of HuR
724 (ELAVL1) at the region that contains the rs13900. **(B)** Predicted changes in the secondary
725 structure using Vienna RNA package 2.0; changes in secondary structure are indicated by
726 arrows. **(C)** Sequence logo of HuR binding site as determined by HOMER. **(D)** Relative
727 structural preference of HuR to different structural contexts, the letters P, L, U, M indicate that
728 the nucleotide is paired (P), in a hairpin loop (L), in an unstructured (or external) region (U),
729 and Miscellaneous (M) region.
730
731 **Figure 4. The rs13900 T allele shows increased in vitro binding of HuR. (A)** REMSA with
732 labelled oligoribonucleotide containing either rs13900 C or T allele and whole cell extracts
733 from 293T cells. § denotes free probe; black arrow, bound probe; red arrow, supershift. **(B)**
734 Representative quantitative densitometric analysis of the antibody shifted complexes
735 suggested increased HuR binding to the oligoribonucleotide bearing rs13900 T allele. The
736 signals in the bound fraction(s) were normalized using the free probe (N = 4). The top panel
737 represents the data from four independent experiments (mean ± SEM). Statistical analyses
738 were performed using Student's t test ($^{*}P$ < 0.001). The bottom panel shows the relative fold
739 enrichment of the bound protein complexes to the oligoribonucleotide containing the rs13900
740 T allele relative to that containing the rs13900 C allele . Statistical significance was calculated
741 using Student t test ($^{*}P$ < 0.001) **(C)** REMSA with labelled oligoribonucleotides containing
742 either rs13900 T or C allele and purified HuR protein. **(D)** Plot showing the fraction of bound
743 rs13900 C or rs13900 T oligoribonucleotides with increasing HuR concentration.
744

745 **Figure 5. rs13900 C and T alleles are associated with differential binding to HuR ex vivo.**
746 **(A)** HuR enrichment in immunoprecipitated material from macrophages stimulated with LPS.
747 **(B)** *CCL2* 3′ UTR was detected at significant levels in the samples precipitated by α-HuR
748 antibody when compared to the control IgG. **(C)** *CCL2* mRNA expression in anti-HuR antibody
749 enriched immunoprecipitated material analyzed by RT-qPCR (N = 4). Statistical significance
750 was calculated using Student t-test (**P* < 0.005). The error bars represent SEM. **(D)** Relative
751 expression levels for rs13900 C and T alleles in macrophages stimulated with LPS (N = 4).
752 Statistical significance was calculated using a Student t-test (**P* < 0.005).
753
754 **Figure 6. Differential effects of rs13900 alleles in reporter assays and role of HuR. (A)**
755 Schematic representation of the luciferase reporter vectors containing *CCL2* 3' UTR with either
756 rs13900 C or T allele. **(B)** HEK-293 cells were transfected with the equal quantities of *CCL2*
757 3′ UTR reporter vectors and luciferase activity was measured 48 hrs later. The relative
758 luciferase activities of the 3′ UTR reporter plasmids were expressed as percent reduction in
759 the luminescence when compared to the control vector that was set to 100% after normalizing
760 for the protein content of the lysates. The error bars indicate the standard error of mean and
761 statistical significance was calculated using two-tailed Student's *t* test (**P* < 0.05). **(C)** HEK-
762 293T cells were transfected with either pCMV6-HuR (0.5 µg) or pCMV-Entry (0.5 µg) and after
763 72 hours they were co-transfected with the two plasmid constructs (0.5 µg). Twenty-four hours
764 after transfection the relative change in luciferase activity was determined. **(D)** Cells were co-
765 transfected with 125 pmol HuR siRNA or control siRNA and with the two plasmid constructs
766 (0.5 µg). Twenty-four hours after transfection the relative change in luciferase activity was
767 determined (normalized to total protein concentration, data from four independent
768 experiments (mean ± SEM; N = 4). Statistical analyses were performed using Fisher LSD
769 method (**P* < 0.05).
770
771 **Figure 7. Influence of rs13900 C and T alleles on *CCL2* translatability. (A)** HEK-293 cells
772 were transfected by nucleofection with control and *CCL2* 3′ UTR reporter constructs with

773 rs13900 C and T alleles. The nucleofected cells were plated separately and harvested for total
774 RNA isolation or lysed for mRNA level or protein level expression of luciferase respectively
775 after 24 h. The reporter mRNA levels from the transfected 293 T cells were quantified by qRT-
776 PCR, and 18S rRNA was used for normalization. **(B)** The relative luciferase activities of the 3′
777 UTR reporter plasmids were expressed as a percentage reduction in the luminescence when
778 compared to the control vector that was set to 100% after normalizing for the protein content
779 of the lysates. **(C)** mRNA translatability was calculated as luciferase activity normalized by the
780 reporter luciferase mRNA level. The error bars indicate the standard error of mean from six
781 independent experiments (N = 6) and statistical significance was calculated using ANOVA and
782 post hoc contrast with Fisher LSD method. (*$P < 0.05$, **$P < 0.005$).

783 **Figure 8. HuR differentially regulates *CCL2* haplotypes. (A)** HuR expression in primary
784 human macrophages following lentiviral transduction. Macrophages obtained from four
785 individuals who are homozygous for either rs13900 C or rs13900 T allele were transduced
786 with either CMV-null or HuR expressing lentiviral particles (pCMV6-HuR) for 72 hours followed
787 by LPS stimulation for 3 h. **(B)** *CCL2* expression determined by RT-qPCR. Error bars
788 represent SEM. Statistical analyses were performed using Student's t test (* $P < 0.05$).

789

790 **Description of the supplemental data**

791 The Supplemental data includes Supplementary Tables 1-4 and Figures S1-S7.

792 **Figure S1. SNP genotyping for rs13900 using TaqMan technology. (A)** Real-time
793 multicomponent amplification curves for the TaqMan's rs13900 assay. Fluorescence signal
794 detected for individuals with rs13900T, rs13900C and rs13900CT genotypes. The blue curve
795 indicates amplification of T allele (alternate/mutant allele) while the green curve represents C
796 allele (wild type). **(B)** Allelic discrimination plot generated on Quant Studio 12K Flex Real-Time
797 PCR system showing higher signal and better cluster separation for the rs13900 assay. Allele
798 C is plotted on X-axis and the T allele is plotted on Y-axis.

799 **Figure S2. Time course of *CCL2* mRNA expression in PBMCs.** Peripheral blood
800 mononuclear cells (PBMC) were treated with 1 µg lipopolysaccharide (LPS) for 1, 3 or 6 hours.
801 *CCL2* mRNA expression was measured by quantitative real-time PCR and normalized to 18S
802 rRNA. Data are presented as mean ± SD of triplicate samples.

803 **Figure S3. Validation of HuR overexpression and silencing by Western blotting. (A)** A
804 representative western blot showing HuR protein levels in HEK293 cells transfected with either
805 pCMV6-HuR plasmid or HuR-targeting siRNA (HuR-siRNA). **(B)** Densitometric analysis of
806 Western blot bands. The histogram shows relative intensity of HuR bands in each sample,
807 normalized to β-actin. Error bar represents standard error mean from three independent
808 experiments. *$p<0.025$, ** $p<0.05$.

809 **Figure S4. Polysomal association of *CCL2* mRNA before and after LPS stimulation of**
810 **macrophages (A)** Polysome profile obtained by sucrose gradient centrifugation from
811 macrophages before and after stimulation with LPS (1 µg/mL) for 3 h. The polysome profile
812 shows a shift from monosome to heavier polysome upon LPS stimulation, indicating active
813 translation. **(B)** The percentage of *CCL2* mRNA loading on polysome fraction was calculated
814 using ΔCT method (mean ± SEM, n=4). *$p<0.025$.

815 **Figure S5. Transduction efficiency of pCMV6-HuR.** Flow-cytometric analysis of
816 transduction efficiency (Panel A) and the intensity of GFP in transduced cells (Panel B).

817 **Figure S6. Flow cytometry analysis of cell surface markers to assess the purity of**
818 **monocytes isolated from PBMC and in vitro differentiation to macrophages. (A)** A
819 representative image depicting the purity of monocytes isolated from PBMCs by
820 immunomagnetic negative selection. A high monocyte content (>90%) was achieved in the
821 enriched fraction. **(B)** Multicolor flow cytometry to determine macrophage differentiation. The
822 macrophage population was identified by forward and side scatter and immunostaining.
823 Surface expressions of CD11c, CD206, CD200, CD16 and CD14 were measured.

824 **Figure S7. Lentiviral transduction of differentiated macrophages.** The differentiation of
825 monocytes into macrophages and their transduction was confirmed by detection of GFP and
826 the cell surface markers CD44, CD200, CD206 by flow cytometry. Cells were transduced with
827 either GFP-tagged pCMV-null **(A)** or GFP-tagged pCMV-HuR particles at MOI of 1 **(B)**. Each
828 bracketed region in the histogram corresponds to the % of positive cells for respective markers
829 noted on the x-axis of the histogram.

830

831 **Supplementary Table 1**. Allele carriages and allele frequencies of rs13900 in healthy
832 volunteers, MAF, minor allele frequency.

833 **Supplementary Table 2**. **Supplementary Table 2.** Crosslinking immunoprecipitation (CLIP)
834 analysis of HuR binding sites on the 3'untranslated region (3'UTR) of the *CCL2* gene.
835 Summary of the SNPs located within HuR-binding regions is shown including SNP ID (rs#),
836 genomic coordinates, strand, binding score, conservation scores (PhastCons, PhyloP),
837 dataset accession numbers, alleles, and SNP position within peak region. Data was generated
838 using POSTAR3 using the variation module.

839 **Supplementary Table 3.** Loading of rs13900 alleles to cytosolic, monosomal and polysomal
840 fractions from macrophage extracts prepared from heterozygous donors. A T:C ratio > 1
841 indicates increased levels of the T allele relative to C allele.

842 **Supplementary Table 4.** Reagents used in the study with source and catalog numbers.

Funding

This research was supported by National Institute of Allergy and Infectious Diseases (NIAID) of the National Institute of Health grant 5R01AI119131. The content is solely the responsibility of the authors and does not necessarily represent the official views of NIAID

Declaration of interests

The authors declare no competing interests.

877 **Web resources**

878 AURA, http://aura.science.unitn.it/

879 POSTAR3, http://postar.ncrnalab.org

880 RBP-var2, http://159.226.67.237/sun/RBP-Var/index.php/Rbp/index

881 ViennaRNA package, https://www.tbi.univie.ac.at/RNA/

882 **References**

883 Akdeli, N., Riemann, K., Westphal, J., Hess, J., Siffert, W., Bachmann, H.S., 2014. A 3'UTR
884 polymorphism modulates mRNA stability of the oncogene and drug target Polo-like Kinase 1.
885 Mol Cancer 13, 87.
886 Alasoo, K., Rodrigues, J., Mukhopadhyay, S., Knights, A.J., Mann, A.L., Kundu, K.,
887 Consortium, H., Hale, C., Dougan, G., Gaffney, D.J., 2018. Shared genetic effects on
888 chromatin and gene expression indicate a role for enhancer priming in immune response.
889 Nat Genet 50, 424-431.
890 Alonso-Villaverde, C., Coll, B., Parra, S., Montero, M., Calvo, N., Tous, M., Joven, J.,
891 Masana, L., 2004. Atherosclerosis in patients infected with HIV is influenced by a mutant
892 monocyte chemoattractant protein-1 allele. Circulation 110, 2204-2209.
893 Anderson, P., 2010. Post-transcriptional regulons coordinate the initiation and resolution of
894 inflammation. Nat Rev Immunol 10, 24-35.
895 Bonello, G.B., Pham, M.H., Begum, K., Sigala, J., Sataranatarajan, K., Mummidi, S., 2011.
896 An evolutionarily conserved TNF-alpha-responsive enhancer in the far upstream region of
897 human CCL2 locus influences its gene expression. J Immunol 186, 7025-7038.
898 Buccitelli, C., Selbach, M., 2020. mRNAs, proteins and the emerging principles of gene
899 expression control. Nat Rev Genet 21, 630-644.
900 Buniello, A., MacArthur, J.A.L., Cerezo, M., Harris, L.W., Hayhurst, J., Malangone, C.,
901 McMahon, A., Morales, J., Mountjoy, E., Sollis, E., Suveges, D., Vrousgou, O., Whetzel,
902 P.L., Amode, R., Guillen, J.A., Riat, H.S., Trevanion, S.J., Hall, P., Junkins, H., Flicek, P.,
903 Burdett, T., Hindorff, L.A., Cunningham, F., Parkinson, H., 2019. The NHGRI-EBI GWAS
904 Catalog of published genome-wide association studies, targeted arrays and summary
905 statistics 2019. Nucleic Acids Res 47, D1005-D1012.
906 Cavestro, G.M., Zuppardo, R.A., Bertolini, S., Sereni, G., Frulloni, L., Okolicsanyi, S.,
907 Calzolari, C., Singh, S.K., Sianesi, M., Del Rio, P., Leandro, G., Franze, A., Di Mario, F.,
908 2010. Connections between genetics and clinical data: Role of MCP-1, CFTR, and SPINK-1
909 in the setting of acute, acute recurrent, and chronic pancreatitis. Am J Gastroenterol 105,
910 199-206.
911 Chen, S., Deng, C., Hu, C., Li, J., Wen, X., Wu, Z., Li, Y., Zhang, F., Li, Y., 2016. Association
912 of MCP-1-2518A/G polymorphism with susceptibility to autoimmune diseases: a meta-
913 analysis. Clin Rheumatol 35, 1169-1179.
914 Cho, M.L., Kim, J.Y., Ko, H.J., Kim, Y.H., Kim, W.U., Cho, C.S., Kim, H.Y., Hwang, S.Y.,
915 2004. The MCP-1 promoter -2518 polymorphism in Behcet's disease: correlation between
916 allele types, MCP-1 production and clinical symptoms among Korean patients. Autoimmunity
917 37, 77-80.
918 Choi, H.J., Yang, H., Park, S.H., Moon, Y., 2009. HuR/ELAVL1 RNA binding protein
919 modulates interleukin-8 induction by muco-active ribotoxin deoxynivalenol. Toxicol Appl
920 Pharmacol 240, 46-54.
921 Chowdhury, P., Khan, S.A., 2017. Significance of CCL2, CCL5 and CCR2 polymorphisms
922 for adverse prognosis of Japanese encephalitis from an endemic population of India. Sci
923 Rep 7, 13716.
924 Darkoh, C., Comer, L., Zewdie, G., Harold, S., Snyder, N., Dupont, H.L., 2014. Chemotactic
925 chemokines are important in the pathogenesis of irritable bowel syndrome. PLoS One 9,
926 e93144.
927 Dassi, E., Re, A., Leo, S., Tebaldi, T., Pasini, L., Peroni, D., Quattrone, A., 2014. AURA 2:
928 Empowering discovery of post-transcriptional networks. Translation (Austin) 2, e27738.
929 de Lange, K.M., Moutsianas, L., Lee, J.C., Lamb, C.A., Luo, Y., Kennedy, N.A., Jostins, L.,
930 Rice, D.L., Gutierrez-Achury, J., Ji, S.G., Heap, G., Nimmo, E.R., Edwards, C., Henderson,
931 P., Mowat, C., Sanderson, J., Satsangi, J., Simmons, A., Wilson, D.C., Tremelling, M., Hart,
932 A., Mathew, C.G., Newman, W.G., Parkes, M., Lees, C.W., Uhlig, H., Hawkey, C., Prescott,
933 N.J., Ahmad, T., Mansfield, J.C., Anderson, C.A., Barrett, J.C., 2017. Genome-wide
934 association study implicates immune activation of multiple integrin genes in inflammatory
935 bowel disease. Nat Genet 49, 256-261.

936 Deshmane, S.L., Kremlev, S., Amini, S., Sawaya, B.E., 2009. Monocyte chemoattractant
937 protein-1 (MCP-1): an overview. J Interferon Cytokine Res 29, 313-326.
938 Duan, J., Shi, J., Ge, X., Dolken, L., Moy, W., He, D., Shi, S., Sanders, A.R., Ross, J.,
939 Gejman, P.V., 2013. Genome-wide survey of interindividual differences of RNA stability in
940 human lymphoblastoid cell lines. Sci Rep 3, 1318.
941 Fan, J., Ishmael, F.T., Fang, X., Myers, A., Cheadle, C., Huang, S.K., Atasoy, U., Gorospe,
942 M., Stellato, C., 2011. Chemokine transcripts as targets of the RNA-binding protein HuR in
943 human airway epithelium. J Immunol 186, 2482-2494.
944 Farh, K.K., Marson, A., Zhu, J., Kleinewietfeld, M., Housley, W.J., Beik, S., Shoresh, N.,
945 Whitton, H., Ryan, R.J., Shishkin, A.A., Hatan, M., Carrasco-Alfonso, M.J., Mayer, D.,
946 Luckey, C.J., Patsopoulos, N.A., De Jager, P.L., Kuchroo, V.K., Epstein, C.B., Daly, M.J.,
947 Hafler, D.A., Bernstein, B.E., 2015. Genetic and epigenetic fine mapping of causal
948 autoimmune disease variants. Nature 518, 337-343.
949 Farr, A., Roman, A., 1992. A pitfall of using a second plasmid to determine transfection
950 efficiency. Nucleic Acids Res 20, 920.
951 Fenoglio, C., Galimberti, D., Lovati, C., Guidi, I., Gatti, A., Fogliarino, S., Tiriticco, M.,
952 Mariani, C., Forloni, G., Pettenati, C., Baron, P., Conti, G., Bresolin, N., Scarpini, E., 2004.
953 MCP-1 in Alzheimer's disease patients: A-2518G polymorphism and serum levels. Neurobiol
954 Aging 25, 1169-1173.
955 Flores-Villanueva, P.O., Ruiz-Morales, J.A., Song, C.H., Flores, L.M., Jo, E.K., Montano, M.,
956 Barnes, P.F., Selman, M., Granados, J., 2005. A functional promoter polymorphism in
957 monocyte chemoattractant protein-1 is associated with increased susceptibility to pulmonary
958 tuberculosis. J Exp Med 202, 1649-1658.
959 Franke, A., McGovern, D.P., Barrett, J.C., Wang, K., Radford-Smith, G.L., Ahmad, T., Lees,
960 C.W., Balschun, T., Lee, J., Roberts, R., Anderson, C.A., Bis, J.C., Bumpstead, S.,
961 Ellinghaus, D., Festen, E.M., Georges, M., Green, T., Haritunians, T., Jostins, L., Latiano, A.,
962 Mathew, C.G., Montgomery, G.W., Prescott, N.J., Raychaudhuri, S., Rotter, J.I., Schumm,
963 P., Sharma, Y., Simms, L.A., Taylor, K.D., Whiteman, D., Wijmenga, C., Baldassano, R.N.,
964 Barclay, M., Bayless, T.M., Brand, S., Buning, C., Cohen, A., Colombel, J.F., Cottone, M.,
965 Stronati, L., Denson, T., De Vos, M., D'Inca, R., Dubinsky, M., Edwards, C., Florin, T.,
966 Franchimont, D., Gearry, R., Glas, J., Van Gossum, A., Guthery, S.L., Halfvarson, J.,
967 Verspaget, H.W., Hugot, J.P., Karban, A., Laukens, D., Lawrance, I., Lemann, M., Levine,
968 A., Libioulle, C., Louis, E., Mowat, C., Newman, W., Panes, J., Phillips, A., Proctor, D.D.,
969 Regueiro, M., Russell, R., Rutgeerts, P., Sanderson, J., Sans, M., Seibold, F., Steinhart,
970 A.H., Stokkers, P.C., Torkvist, L., Kullak-Ublick, G., Wilson, D., Walters, T., Targan, S.R.,
971 Brant, S.R., Rioux, J.D., D'Amato, M., Weersma, R.K., Kugathasan, S., Griffiths, A.M.,
972 Mansfield, J.C., Vermeire, S., Duerr, R.H., Silverberg, M.S., Satsangi, J., Schreiber, S., Cho,
973 J.H., Annese, V., Hakonarson, H., Daly, M.J., Parkes, M., 2010. Genome-wide meta-
974 analysis increases to 71 the number of confirmed Crohn's disease susceptibility loci. Nat
975 Genet 42, 1118-1125.
976 Ge, B., Gurd, S., Gaudin, T., Dore, C., Lepage, P., Harmsen, E., Hudson, T.J., Pastinen, T.,
977 2005. Survey of allelic expression using EST mining. Genome Res 15, 1584-1591.
978 Glisovic, T., Bachorik, J.L., Yong, J., Dreyfuss, G., 2008. RNA-binding proteins and post-
979 transcriptional gene regulation. FEBS Lett 582, 1977-1986.
980 Gonzalez, E., Rovin, B.H., Sen, L., Cooke, G., Dhanda, R., Mummidi, S., Kulkarni, H.,
981 Bamshad, M.J., Telles, V., Anderson, S.A., Walter, E.A., Stephan, K.T., Deucher, M.,
982 Mangano, A., Bologna, R., Ahuja, S.S., Dolan, M.J., Ahuja, S.K., 2002. HIV-1 infection and
983 AIDS dementia are influenced by a mutant MCP-1 allele linked to increased monocyte
984 infiltration of tissues and MCP-1 levels. Proc Natl Acad Sci U S A 99, 13795-13800.
985 Gschwandtner, M., Derler, R., Midwood, K.S., 2019. More Than Just Attractive: How CCL2
986 Influences Myeloid Cell Behavior Beyond Chemotaxis. Front Immunol 10, 2759.
987 Hao, S., Baltimore, D., 2009. The stability of mRNA influences the temporal order of the
988 induction of genes encoding inflammatory molecules. Nat Immunol 10, 281-288.
989 Heinz, S., Benner, C., Spann, N., Bertolino, E., Lin, Y.C., Laslo, P., Cheng, J.X., Murre, C.,
990 Singh, H., Glass, C.K., 2010. Simple combinations of lineage-determining transcription

991 factors prime cis-regulatory elements required for macrophage and B cell identities. Mol Cell
992 38, 576-589.
993 Hollander, D., Naftelberg, S., Lev-Maor, G., Kornblihtt, A.R., Ast, G., 2016. How Are Short
994 Exons Flanked by Long Introns Defined and Committed to Splicing? Trends Genet 32, 596-
995 606.
996 Huang, Z., Shi, J., Gao, Y., Cui, C., Zhang, S., Li, J., Zhou, Y., Cui, Q., 2019. HMDD v3.0: a
997 database for experimentally supported human microRNA-disease associations. Nucleic
998 Acids Res 47, D1013-D1017.
999 Hubal, M.J., Devaney, J.M., Hoffman, E.P., Zambraski, E.J., Gordish-Dressman, H., Kearns,
1000 A.K., Larkin, J.S., Adham, K., Patel, R.R., Clarkson, P.M., 2010. CCL2 and CCR2
1001 polymorphisms are associated with markers of exercise-induced skeletal muscle damage. J
1002 Appl Physiol (1985) 108, 1651-1658.
1003 Intemann, C.D., Thye, T., Forster, B., Owusu-Dabo, E., Gyapong, J., Horstmann, R.D.,
1004 Meyer, C.G., 2011. MCP1 haplotypes associated with protection from pulmonary
1005 tuberculosis. BMC Genet 12, 34.
1006 Jao, C.Y., Salic, A., 2008. Exploring RNA transcription and turnover in vivo by using click
1007 chemistry. Proc Natl Acad Sci U S A 105, 15779-15784.
1008 Johnson, A.D., Zhang, Y., Papp, A.C., Pinsonneault, J.K., Lim, J.E., Saffen, D., Dai, Z.,
1009 Wang, D., Sadee, W., 2008. Polymorphisms affecting gene transcription and mRNA
1010 processing in pharmacogenetic candidate genes: detection through allelic expression
1011 imbalance in human target tissues. Pharmacogenet Genomics 18, 781-791.
1012 Joven, J., Coll, B., Tous, M., Ferre, N., Alonso-Villaverde, C., Parra, S., Camps, J., 2006.
1013 The influence of HIV infection on the correlation between plasma concentrations of
1014 monocyte chemoattractant protein-1 and carotid atherosclerosis. Clin Chim Acta 368, 114-
1015 119.
1016 Kasztelewicz, B., Czech-Kowalska, J., Lipka, B., Milewska-Bobula, B., Borszewska-
1017 Kornacka, M.K., Romanska, J., Dzierzanowska-Fangrat, K., 2017. Cytokine gene
1018 polymorphism associations with congenital cytomegalovirus infection and sensorineural
1019 hearing loss. Eur J Clin Microbiol Infect Dis 36, 1811-1818.
1020 Kazan, H., Ray, D., Chan, E.T., Hughes, T.R., Morris, Q., 2010. RNAcontext: a new method
1021 for learning the sequence and structure binding preferences of RNA-binding proteins. PLoS
1022 Comput Biol 6, e1000832.
1023 Kenny, E.E., Pe'er, I., Karban, A., Ozelius, L., Mitchell, A.A., Ng, S.M., Erazo, M., Ostrer, H.,
1024 Abraham, C., Abreu, M.T., Atzmon, G., Barzilai, N., Brant, S.R., Bressman, S., Burns, E.R.,
1025 Chowers, Y., Clark, L.N., Darvasi, A., Doheny, D., Duerr, R.H., Eliakim, R., Giladi, N.,
1026 Gregersen, P.K., Hakonarson, H., Jones, M.R., Marder, K., McGovern, D.P., Mulle, J., Orr-
1027 Urtreger, A., Proctor, D.D., Pulver, A., Rotter, J.I., Silverberg, M.S., Ullman, T., Warren, S.T.,
1028 Waterman, M., Zhang, W., Bergman, A., Mayer, L., Katz, S., Desnick, R.J., Cho, J.H., Peter,
1029 I., 2012. A genome-wide scan of Ashkenazi Jewish Crohn's disease suggests novel
1030 susceptibility loci. PLoS Genet 8, e1002559.
1031 Kim, S., Kim, S., Chang, H.R., Kim, D., Park, J., Son, N., Park, J., Yoon, M., Chae, G., Kim,
1032 Y.K., Kim, V.N., Kim, Y.K., Nam, J.W., Shin, C., Baek, D., 2021. The regulatory impact of
1033 RNA-binding proteins on microRNA targeting. Nat Commun 12, 5057.
1034 Kwong, A., Boughton, A.P., Wang, M., VandeHaar, P., Boehnke, M., Abecasis, G., Kang,
1035 H.M., 2021. FIVEx: an interactive eQTL browser across public datasets. Bioinformatics.
1036 Lebedeva, S., Jens, M., Theil, K., Schwanhausser, B., Selbach, M., Landthaler, M.,
1037 Rajewsky, N., 2011. Transcriptome-wide analysis of regulatory interactions of the RNA-
1038 binding protein HuR. Mol Cell 43, 340-352.
1039 Letendre, S., Marquie-Beck, J., Singh, K.K., de Almeida, S., Zimmerman, J., Spector, S.A.,
1040 Grant, I., Ellis, R., Group, H., 2004. The monocyte chemotactic protein-1 -2578G allele is
1041 associated with elevated MCP-1 concentrations in cerebrospinal fluid. J Neuroimmunol 157,
1042 193-196.
1043 Li, Y.I., van de Geijn, B., Raj, A., Knowles, D.A., Petti, A.A., Golan, D., Gilad, Y., Pritchard,
1044 J.K., 2016. RNA splicing is a primary link between genetic variation and disease. Science
1045 352, 600-604.

1046 Liu, J.Z., van Sommeren, S., Huang, H., Ng, S.C., Alberts, R., Takahashi, A., Ripke, S., Lee,
1047 J.C., Jostins, L., Shah, T., Abedian, S., Cheon, J.H., Cho, J., Dayani, N.E., Franke, L.,
1048 Fuyuno, Y., Hart, A., Juyal, R.C., Juyal, G., Kim, W.H., Morris, A.P., Poustchi, H., Newman,
1049 W.G., Midha, V., Orchard, T.R., Vahedi, H., Sood, A., Sung, J.Y., Malekzadeh, R., Westra,
1050 H.J., Yamazaki, K., Yang, S.K., International Multiple Sclerosis Genetics, C., International,
1051 I.B.D.G.C., Barrett, J.C., Alizadeh, B.Z., Parkes, M., Bk, T., Daly, M.J., Kubo, M., Anderson,
1052 C.A., Weersma, R.K., 2015. Association analyses identify 38 susceptibility loci for
1053 inflammatory bowel disease and highlight shared genetic risk across populations. Nat Genet
1054 47, 979-986.
1055 Liu, Y., Beyer, A., Aebersold, R., 2016. On the Dependency of Cellular Protein Levels on
1056 mRNA Abundance. Cell 165, 535-550.
1057 Lorenz, R., Bernhart, S.H., Honer Zu Siederdissen, C., Tafer, H., Flamm, C., Stadler, P.F.,
1058 Hofacker, I.L., 2011. ViennaRNA Package 2.0. Algorithms Mol Biol 6, 26.
1059 MacArthur, J., Bowler, E., Cerezo, M., Gil, L., Hall, P., Hastings, E., Junkins, H., McMahon,
1060 A., Milano, A., Morales, J., Pendlington, Z.M., Welter, D., Burdett, T., Hindorff, L., Flicek, P.,
1061 Cunningham, F., Parkinson, H., 2017. The new NHGRI-EBI Catalog of published genome-
1062 wide association studies (GWAS Catalog). Nucleic Acids Res 45, D896-D901.
1063 Maharshak, N., Hart, G., Ron, E., Zelman, E., Sagiv, A., Arber, N., Brazowski, E., Margalit,
1064 R., Elinav, E., Shachar, I., 2010. CCL2 (pM levels) as a therapeutic agent in Inflammatory
1065 Bowel Disease models in mice. Inflamm Bowel Dis 16, 1496-1504.
1066 Manolio, T.A., 2010. Genomewide association studies and assessment of the risk of
1067 disease. N Engl J Med 363, 166-176.
1068 Mao, F., Xiao, L., Li, X., Liang, J., Teng, H., Cai, W., Sun, Z.S., 2016. RBP-Var: a database
1069 of functional variants involved in regulation mediated by RNA-binding proteins. Nucleic Acids
1070 Res 44, D154-163.
1071 Martin, J.C., Chang, C., Boschetti, G., Ungaro, R., Giri, M., Grout, J.A., Gettler, K., Chuang,
1072 L.S., Nayar, S., Greenstein, A.J., Dubinsky, M., Walker, L., Leader, A., Fine, J.S.,
1073 Whitehurst, C.E., Mbow, M.L., Kugathasan, S., Denson, L.A., Hyams, J.S., Friedman, J.R.,
1074 Desai, P.T., Ko, H.M., Laface, I., Akturk, G., Schadt, E.E., Salmon, H., Gnjatic, S., Rahman,
1075 A.H., Merad, M., Cho, J.H., Kenigsberg, E., 2019. Single-Cell Analysis of Crohn's Disease
1076 Lesions Identifies a Pathogenic Cellular Module Associated with Resistance to Anti-TNF
1077 Therapy. Cell 178, 1493-1508 e1420.
1078 Matsumiya, T., Ota, K., Imaizumi, T., Yoshida, H., Kimura, H., Satoh, K., 2010.
1079 Characterization of synergistic induction of CX3CL1/fractalkine by TNF-alpha and IFN-
1080 gamma in vascular endothelial cells: an essential role for TNF-alpha in post-transcriptional
1081 regulation of CX3CL1. J Immunol 184, 4205-4214.
1082 Maurano, M.T., Humbert, R., Rynes, E., Thurman, R.E., Haugen, E., Wang, H., Reynolds,
1083 A.P., Sandstrom, R., Qu, H., Brody, J., Shafer, A., Neri, F., Lee, K., Kutyavin, T., Stehling-
1084 Sun, S., Johnson, A.K., Canfield, T.K., Giste, E., Diegel, M., Bates, D., Hansen, R.S., Neph,
1085 S., Sabo, P.J., Heimfeld, S., Raubitschek, A., Ziegler, S., Cotsapas, C., Sotoodehnia, N.,
1086 Glass, I., Sunyaev, S.R., Kaul, R., Stamatoyannopoulos, J.A., 2012. Systematic localization
1087 of common disease-associated variation in regulatory DNA. Science 337, 1190-1195.
1088 Mayr, C., 2019. What Are 3' UTRs Doing? Cold Spring Harb Perspect Biol 11.
1089 McDermott, D.H., Yang, Q., Kathiresan, S., Cupples, L.A., Massaro, J.M., Keaney, J.F., Jr.,
1090 Larson, M.G., Vasan, R.S., Hirschhorn, J.N., O'Donnell, C.J., Murphy, P.M., Benjamin, E.J.,
1091 2005. CCL2 polymorphisms are associated with serum monocyte chemoattractant protein-1
1092 levels and myocardial infarction in the Framingham Heart Study. Circulation 112, 1113-1120.
1093 Melgarejo, E., Medina, M.A., Sanchez-Jimenez, F., Urdiales, J.L., 2009. Monocyte
1094 chemoattractant protein-1: a key mediator in inflammatory processes. Int J Biochem Cell Biol
1095 41, 998-1001.
1096 Morrison, A.R., Yarovinsky, T.O., Young, B.D., Moraes, F., Ross, T.D., Ceneri, N., Zhang, J.,
1097 Zhuang, Z.W., Sinusas, A.J., Pardi, R., Schwartz, M.A., Simons, M., Bender, J.R., 2014.
1098 Chemokine-coupled beta2 integrin-induced macrophage Rac2-Myosin IIA interaction
1099 regulates VEGF-A mRNA stability and arteriogenesis. J Exp Med 211, 1957-1968.

1100 Mummidi, S., Bonello, G.B., Ahuja, S.K., 2009. Confirmation of differential binding of
1101 Interferon Regulatory Factor-1 (IRF-1) to the functional and HIV disease-influencing -2578
1102 A/G polymorphism in CCL2. Genes Immun 10, 197-198; author reply 199.
1103 Nayak, B.K., Feliers, D., Sudarshan, S., Friedrichs, W.E., Day, R.T., New, D.D., Fitzgerald,
1104 J.P., Eid, A., Denapoli, T., Parekh, D.J., Gorin, Y., Block, K., 2013. Stabilization of HIF-
1105 2alpha through redox regulation of mTORC2 activation and initiation of mRNA translation.
1106 Oncogene 32, 3147-3155.
1107 Nedelec, Y., Sanz, J., Baharian, G., Szpiech, Z.A., Pacis, A., Dumaine, A., Grenier, J.C.,
1108 Freiman, A., Sams, A.J., Hebert, S., Page Sabourin, A., Luca, F., Blekhman, R., Hernandez,
1109 R.D., Pique-Regi, R., Tung, J., Yotova, V., Barreiro, L.B., 2016. Genetic Ancestry and
1110 Natural Selection Drive Population Differences in Immune Responses to Pathogens. Cell
1111 167, 657-669 e621.
1112 Pabis, M., Popowicz, G.M., Stehle, R., Fernandez-Ramos, D., Asami, S., Warner, L., Garcia-
1113 Maurino, S.M., Schlundt, A., Martinez-Chantar, M.L., Diaz-Moreno, I., Sattler, M., 2019. HuR
1114 biological function involves RRM3-mediated dimerization and RNA binding by all three
1115 RRMs. Nucleic Acids Res 47, 1011-1029.
1116 Page, S.H., Wright, E.K., Jr., Gama, L., Clements, J.E., 2011. Regulation of CCL2
1117 expression by an upstream TALE homeodomain protein-binding site that synergizes with the
1118 site created by the A-2578G SNP. PLoS One 6, e22052.
1119 Pai, A.A., Cain, C.E., Mizrahi-Man, O., De Leon, S., Lewellen, N., Veyrieras, J.B., Degner,
1120 J.F., Gaffney, D.J., Pickrell, J.K., Stephens, M., Pritchard, J.K., Gilad, Y., 2012. The
1121 contribution of RNA decay quantitative trait loci to inter-individual variation in steady-state
1122 gene expression levels. PLoS Genet 8, e1003000.
1123 Palmieri, O., Latiano, A., Salvatori, E., Valvano, M.R., Bossa, F., Latiano, T., Corritore, G., di
1124 Mauro, L., Andriulli, A., Annesec, V., 2010. The -A2518G polymorphism of monocyte
1125 chemoattractant protein-1 is associated with Crohn's disease. Am J Gastroenterol 105,
1126 1586-1594.
1127 Paulsen, M.T., Veloso, A., Prasad, J., Bedi, K., Ljungman, E.A., Tsan, Y.C., Chang, C.W.,
1128 Tarrier, B., Washburn, J.G., Lyons, R., Robinson, D.R., Kumar-Sinha, C., Wilson, T.E.,
1129 Ljungman, M., 2013. Coordinated regulation of synthesis and stability of RNA during the
1130 acute TNF-induced proinflammatory response. Proc Natl Acad Sci U S A 110, 2240-2245.
1131 Payne, J.L., Khalid, F., Wagner, A., 2018. RNA-mediated gene regulation is less evolvable
1132 than transcriptional regulation. Proc Natl Acad Sci U S A 115, E3481-E3490.
1133 Pham, M.H., Bonello, G.B., Castiblanco, J., Le, T., Sigala, J., He, W., Mummidi, S., 2012.
1134 The rs1024611 regulatory region polymorphism is associated with CCL2 allelic expression
1135 imbalance. PLoS One 7, e49498.
1136 Plaisance-Bonstaff, K., Faia, C., Wyczechowska, D., Jeansonne, D., Vittori, C., Peruzzi, F.,
1137 2019. Isolation, Transfection, and Culture of Primary Human Monocytes. J Vis Exp.
1138 Pullmann, R., Jr., Abdelmohsen, K., Lal, A., Martindale, J.L., Ladner, R.D., Gorospe, M.,
1139 2006. Differential stability of thymidylate synthase 3'-untranslated region polymorphic
1140 variants regulated by AUF1. J Biol Chem 281, 23456-23463.
1141 Quach, H., Rotival, M., Pothlichet, J., Loh, Y.E., Dannemann, M., Zidane, N., Laval, G.,
1142 Patin, E., Harmant, C., Lopez, M., Deschamps, M., Naffakh, N., Duffy, D., Coen, A., Leroux-
1143 Roels, G., Clement, F., Boland, A., Deleuze, J.F., Kelso, J., Albert, M.L., Quintana-Murci, L.,
1144 2016. Genetic Adaptation and Neandertal Admixture Shaped the Immune System of Human
1145 Populations. Cell 167, 643-656 e617.
1146 Rabani, M., Levin, J.Z., Fan, L., Adiconis, X., Raychowdhury, R., Garber, M., Gnirke, A.,
1147 Nusbaum, C., Hacohen, N., Friedman, N., Amit, I., Regev, A., 2011. Metabolic labeling of
1148 RNA uncovers principles of RNA production and degradation dynamics in mammalian cells.
1149 Nat Biotechnol 29, 436-442.
1150 Reyes, R., Alcalde, J., Izquierdo, J.M., 2009. Depletion of T-cell intracellular antigen proteins
1151 promotes cell proliferation. Genome Biol 10, R87.
1152 Ripin, N., Boudet, J., Duszczyk, M.M., Hinniger, A., Faller, M., Krepl, M., Gadi, A.,
1153 Schneider, R.J., Sponer, J., Meisner-Kober, N.C., Allain, F.H., 2019. Molecular basis for AU-

1154 rich element recognition and dimerization by the HuR C-terminal RRM. Proc Natl Acad Sci U
1155 S A 116, 2935-2944.
1156 Ross, J., 1995. mRNA stability in mammalian cells. Microbiol Rev 59, 423-450.
1157 Rovin, B.H., Lu, L., Saxena, R., 1999. A novel polymorphism in the MCP-1 gene regulatory
1158 region that influences MCP-1 expression. Biochem Biophys Res Commun 259, 344-348.
1159 Sasaki, Y., Dehnad, A., Fish, S., Sato, A., Jiang, J., Tian, J., Schroder, K., Brandes, R.,
1160 Torok, N.J., 2017. NOX4 Regulates CCR2 and CCL2 mRNA Stability in Alcoholic Liver
1161 Disease. Sci Rep 7, 46144.
1162 Schott, J., Reitter, S., Philipp, J., Haneke, K., Schafer, H., Stoecklin, G., 2014. Translational
1163 regulation of specific mRNAs controls feedback inhibition and survival during macrophage
1164 activation. PLoS Genet 10, e1004368.
1165 Schultz, C.W., Preet, R., Dhir, T., Dixon, D.A., Brody, J.R., 2020. Understanding and
1166 targeting the disease-related RNA binding protein human antigen R (HuR). Wiley Interdiscip
1167 Rev RNA 11, e1581.
1168 Schwerk, J., Savan, R., 2015. Translating the Untranslated Region. J Immunol 195, 2963-
1169 2971.
1170 Sharif, O., Bolshakov, V.N., Raines, S., Newham, P., Perkins, N.D., 2007. Transcriptional
1171 profiling of the LPS induced NF-kappaB response in macrophages. BMC Immunol 8, 1.
1172 Shatoff, E., Bundschuh, R., 2020. Single nucleotide polymorphisms affect RNA-protein
1173 interactions at a distance through modulation of RNA secondary structures. PLoS Comput
1174 Biol 16, e1007852.
1175 Steri, M., Idda, M.L., Whalen, M.B., Orru, V., 2018. Genetic variants in mRNA untranslated
1176 regions. Wiley Interdiscip Rev RNA 9, e1474.
1177 Szalai, C., Kozma, G.T., Nagy, A., Bojszko, A., Krikovszky, D., Szabo, T., Falus, A., 2001.
1178 Polymorphism in the gene regulatory region of MCP-1 is associated with asthma
1179 susceptibility and severity. J Allergy Clin Immunol 108, 375-381.
1180 Tam, V., Patel, N., Turcotte, M., Bosse, Y., Pare, G., Meyre, D., 2019. Benefits and
1181 limitations of genome-wide association studies. Nat Rev Genet 20, 467-484.
1182 Tu, X., Chong, W.P., Zhai, Y., Zhang, H., Zhang, F., Wang, S., Liu, W., Wei, M., Siu, N.H.,
1183 Yang, H., Yang, W., Cao, W., Lau, Y.L., He, F., Zhou, G., 2015. Functional polymorphisms
1184 of the CCL2 and MBL genes cumulatively increase susceptibility to severe acute respiratory
1185 syndrome coronavirus infection. J Infect 71, 101-109.
1186 Tucci, M., Barnes, E.V., Sobel, E.S., Croker, B.P., Segal, M.S., Reeves, W.H., Richards,
1187 H.B., 2004. Strong association of a functional polymorphism in the monocyte
1188 chemoattractant protein 1 promoter gene with lupus nephritis. Arthritis Rheum 50, 1842-
1189 1849.
1190 Uren, P.J., Burns, S.C., Ruan, J., Singh, K.K., Smith, A.D., Penalva, L.O., 2011. Genomic
1191 analyses of the RNA-binding protein Hu antigen R (HuR) identify a complex network of
1192 target genes and novel characteristics of its binding sites. J Biol Chem 286, 37063-37066.
1193 Vilmundarson, R.O., Duong, A., Soheili, F., Chen, H.H., Stewart, A.F.R., 2021. IRF2BP2
1194 3'UTR Polymorphism Increases Coronary Artery Calcification in Men. Front Cardiovasc Med
1195 8, 687645.
1196 Visscher, P.M., Wray, N.R., Zhang, Q., Sklar, P., McCarthy, M.I., Brown, M.A., Yang, J.,
1197 2017. 10 Years of GWAS Discovery: Biology, Function, and Translation. Am J Hum Genet
1198 101, 5-22.
1199 Wang, J., Pitarque, M., Ingelman-Sundberg, M., 2006. 3'-UTR polymorphism in the human
1200 CYP2A6 gene affects mRNA stability and enzyme expression. Biochem Biophys Res
1201 Commun 340, 491-497.
1202 Wang, Z., Kayikci, M., Briese, M., Zarnack, K., Luscombe, N.M., Rot, G., Zupan, B., Curk, T.,
1203 Ule, J., 2010. iCLIP predicts the dual splicing effects of TIA-RNA interactions. PLoS Biol 8,
1204 e1000530.
1205 Wright, E.K., Jr., Page, S.H., Barber, S.A., Clements, J.E., 2008. Prep1/Pbx2 complexes
1206 regulate CCL2 expression through the -2578 guanine polymorphism. Genes Immun 9, 419-
1207 430.

1208 Wu, X., Brewer, G., 2012. The regulation of mRNA stability in mammalian cells: 2.0. Gene
1209 500, 10-21.
1210 Xia, J., Bogardus, C., Prochazka, M., 1999. A type 2 diabetes-associated polymorphic ARE
1211 motif affecting expression of PPP1R3 is involved in RNA-protein interactions. Mol Genet
1212 Metab 68, 48-55.
1213 Yoshimura, T., Yuhki, N., Moore, S.K., Appella, E., Lerman, M.I., Leonard, E.J., 1989.
1214 Human monocyte chemoattractant protein-1 (MCP-1). Full-length cDNA cloning, expression
1215 in mitogen-stimulated blood mononuclear leukocytes, and sequence similarity to mouse
1216 competence gene JE. FEBS Lett 244, 487-493.
1217 Yoshinaga, M., Takeuchi, O., 2019. Post-transcriptional control of immune responses and its
1218 potential application. Clin Transl Immunology 8, e1063.
1219 Zhai, Y., Zhong, Z., Chen, C.Y., Xia, Z., Song, L., Blackburn, M.R., Shyu, A.B., 2008.
1220 Coordinated changes in mRNA turnover, translation, and RNA processing bodies in
1221 bronchial epithelial cells following inflammatory stimulation. Mol Cell Biol 28, 7414-7426.
1222 Zhang, F., Lupski, J.R., 2015. Non-coding genetic variants in human disease. Hum Mol
1223 Genet 24, R102-110.
1224 Zhang, X., Chen, X., Liu, Q., Zhang, S., Hu, W., 2017. Translation repression via modulation
1225 of the cytoplasmic poly(A)-binding protein in the inflammatory response. Elife 6.
1226 Zhao, W., Zhang, S., Zhu, Y., Xi, X., Bao, P., Ma, Z., Kapral, T.H., Chen, S., Zagrovic, B.,
1227 Yang, Y.T., Lu, Z.J., 2022. POSTAR3: an updated platform for exploring post-transcriptional
1228 regulation coordinated by RNA-binding proteins. Nucleic Acids Res 50, D287-D294.
1229 Zou, J., Hormozdiari, F., Jew, B., Castel, S.E., Lappalainen, T., Ernst, J., Sul, J.H., Eskin, E.,
1230 2019. Leveraging allelic imbalance to refine fine-mapping for eQTL studies. PLoS Genet 15,
1231 e1008481.

1232

Figure 1

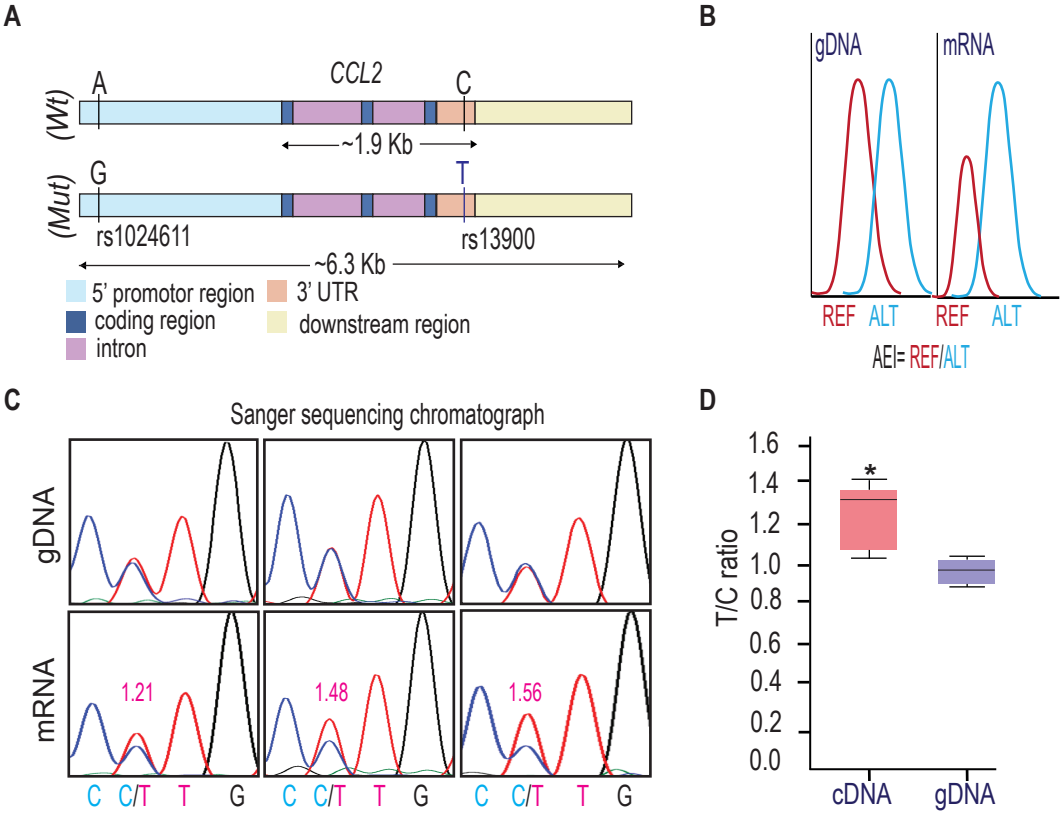
A
CCL2
(Wt)
A
C
~1.9 Kb
(Mut)
G
T
rs1024611
rs13900
~6.3 Kb
5' promotor region
3' UTR
coding region
downstream region
intron
B
gDNA
mRNA
REF
ALT
REF
ALT
AEI= REF/ALT
C
Sanger sequencing chromatograph
gDNA
mRNA
1.21
1.48
1.56
C
C/T
T
G
C
C/T
T
G
C
C/T
T
G
D
T/C ratio
1.6
1.4
1.2
1.0
0.8
0.6
0.4
0.2
0.0
*
cDNA
gDNA

Figure 2

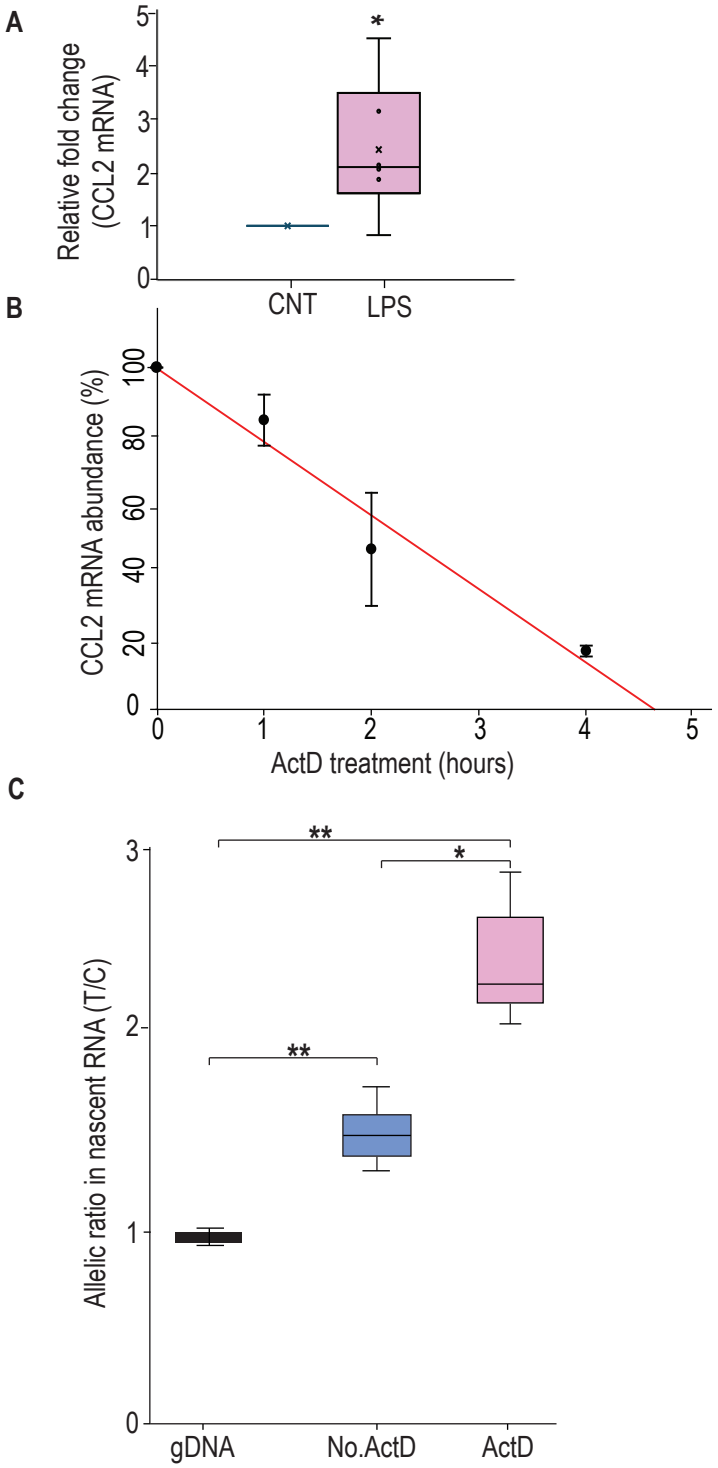
A
Relative fold change (CCL2 mRNA)
5
4
3
2
1
0
*
CNT
LPS
B
CCL2 mRNA abundance (%)
100
80
60
40
20
0
0
1
2
3
4
5
ActD treatment (hours)
C
Allelic ratio in nascent RNA (T/C)
3
2
1
0
**
*
**
gDNA
No.ActD
ActD

Figure 3

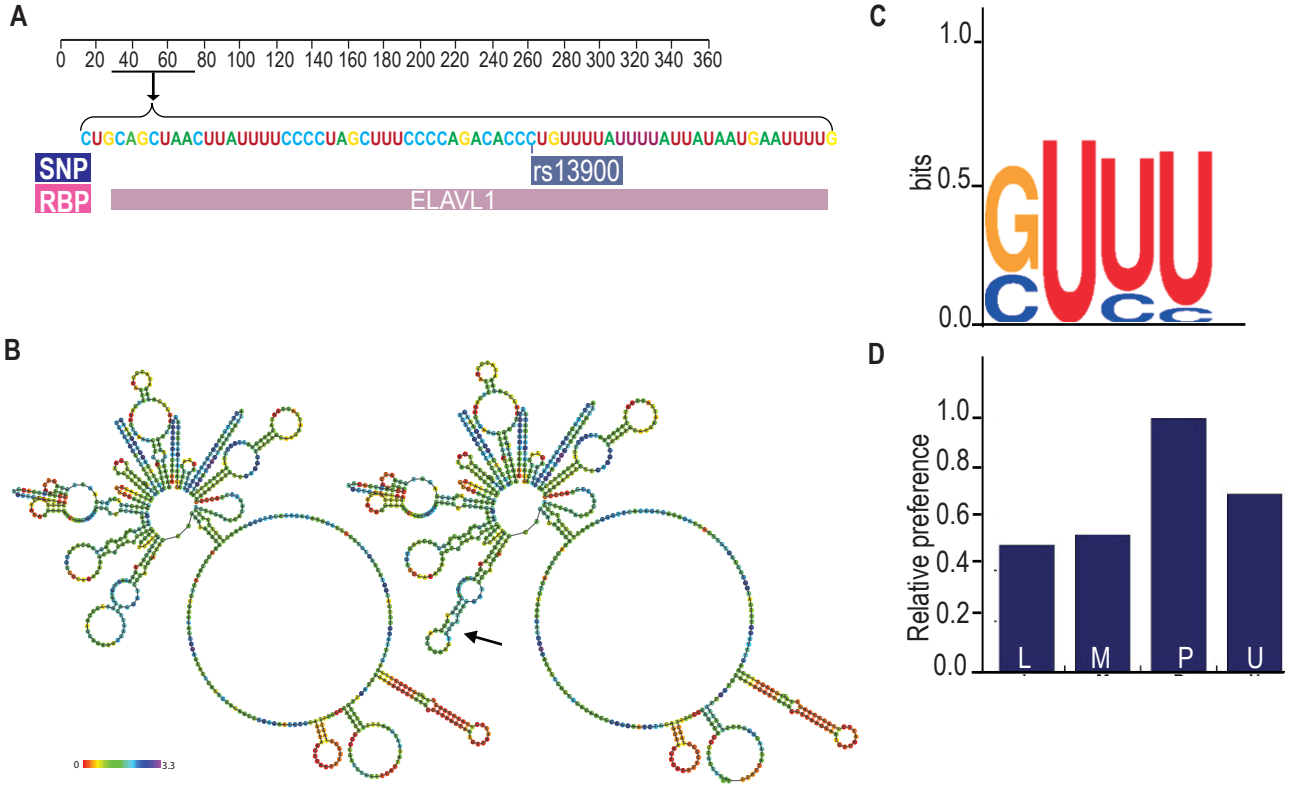
A
0 20 40 60 80 100 120 140 160 180 200 220 240 260 280 300 320 340 360
CUGCAGCUAACUUAUUUUCCCCUAGCUUUCCCCAGACACCCUGUUUUAUUUUAUUAUAAUGAAUUUUG
SNP
rs13900
RBP
ELAVL1
B
0
3.3
C
1.0
bits
0.5
0.0
D
1.0
0.8
0.6
0.4
0.2
0.0
Relative preference
L
M
P
U

Figure 4

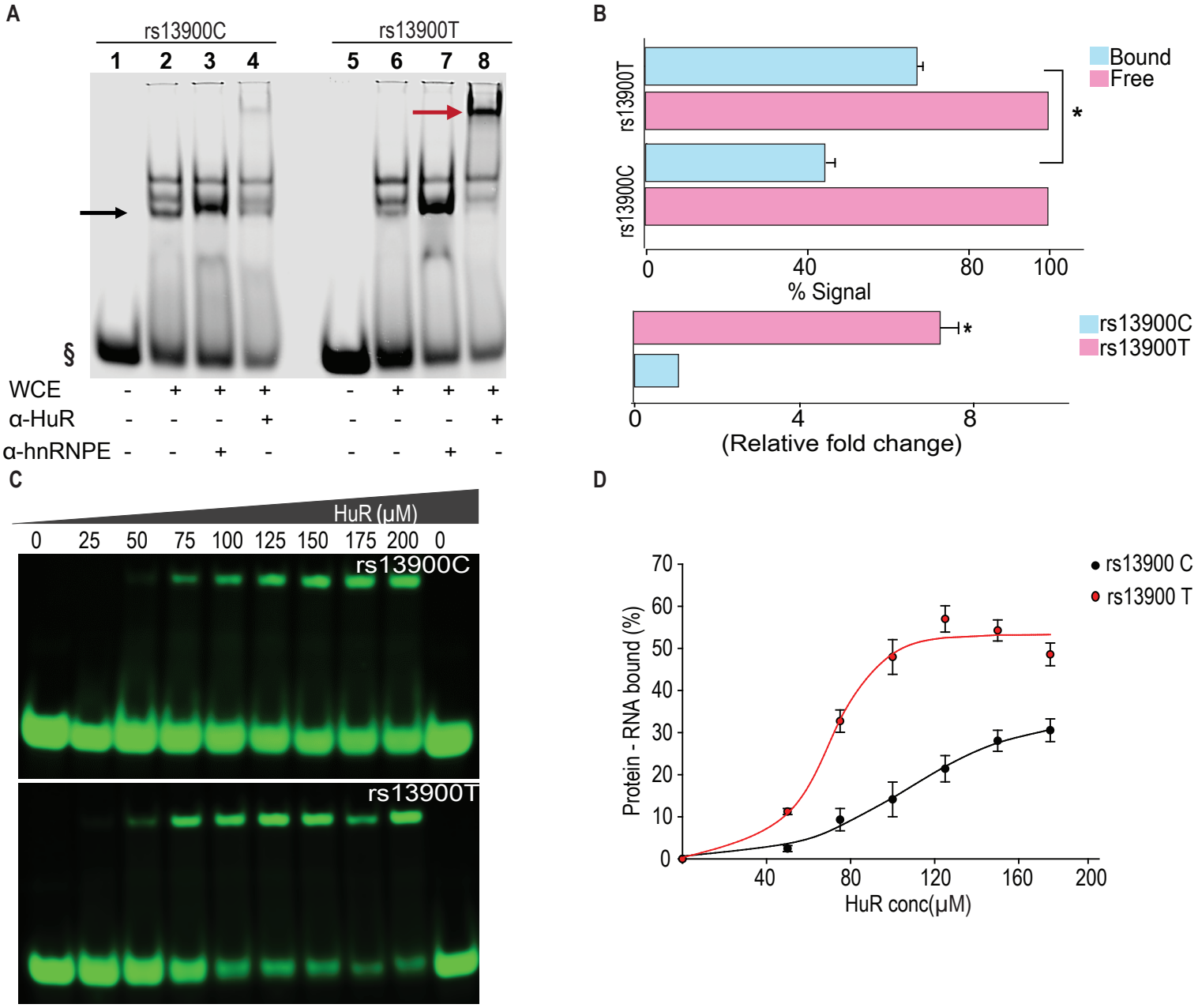
A
rs13900C
rs13900T
1 2 3 4
5 6 7 8
§
WCE - + + + - + + +
α-HuR - - - + - - - +
α-hnRNPE - - + - - - + -
B
Bound
Free
rs13900T
rs13900C
*
0 40 80 100
% Signal
rs13900C
rs13900T
*
0 4 8
(Relative fold change)
C
HuR (μM)
0 25 50 75 100 125 150 175 200 0
rs13900C
rs13900T
D
rs13900 C
rs13900 T
Protein - RNA bound (%)
0 10 20 30 40 50 60 70
40 80 120 160 200
HuR conc(μM)

Figure 5

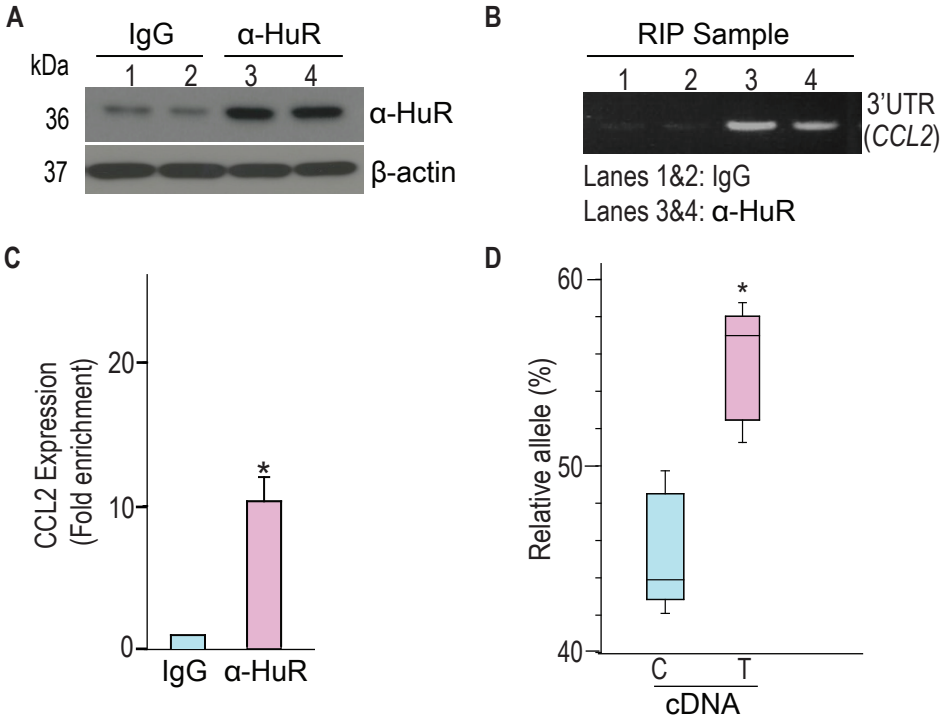
A
IgG
α-HuR
kDa
1
2
3
4
36
α-HuR
37
β-actin
B
RIP Sample
1
2
3
4
3'UTR
(CCL2)
Lanes 1&2: IgG
Lanes 3&4: α-HuR
C
CCL2 Expression
(Fold enrichment)
20
10
0
*
IgG
α-HuR
D
Relative allele (%)
60
50
40
*
C
T
cDNA

Figure 6

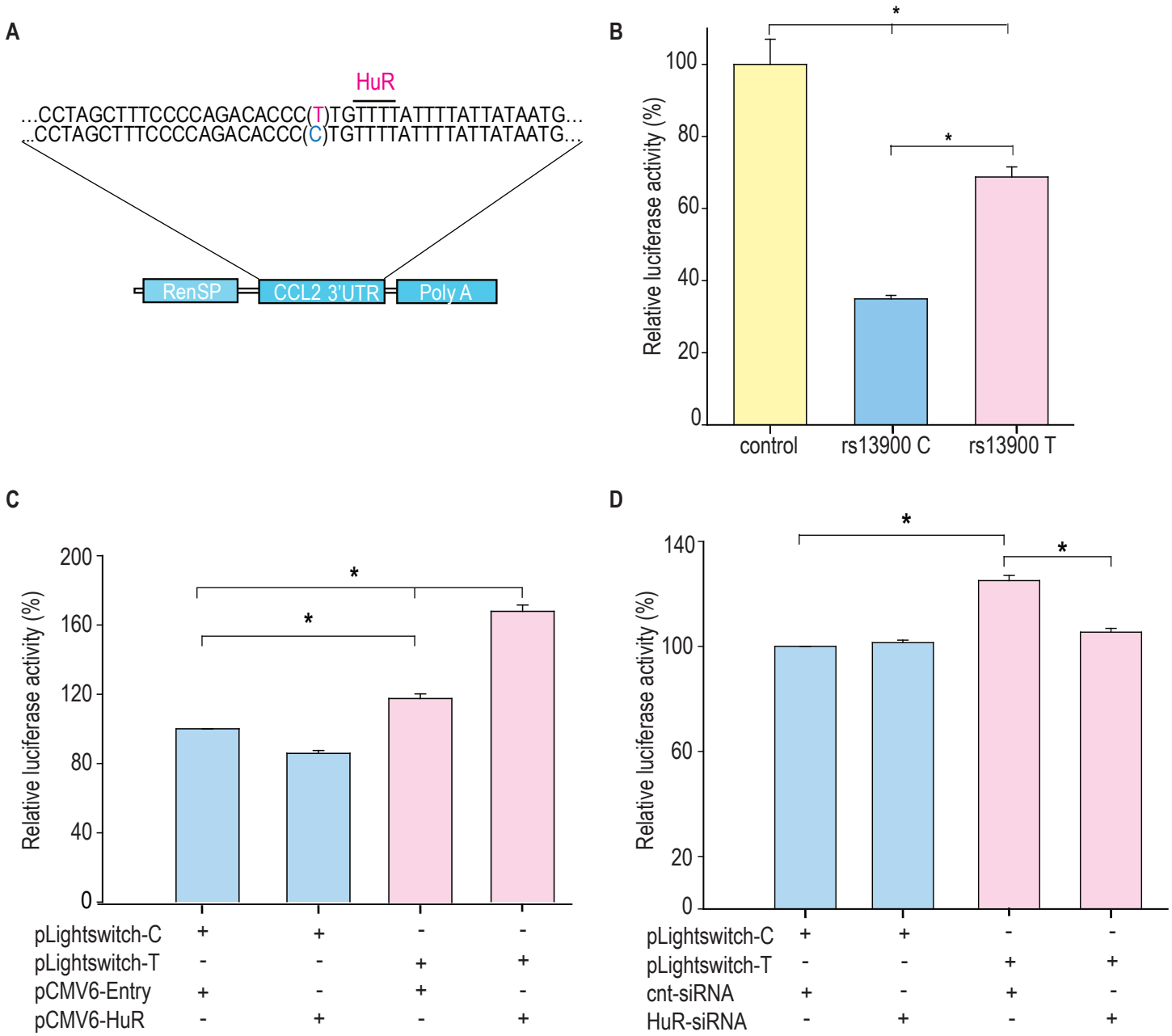
A
HuR
...CCTAGCTTTCCCCAGACACCC(T)TGTTTTATTTTATTATAATG...
...CCTAGCTTTCCCCAGACACCC(C)TGTTTTATTTTATTATAATG...
RenSP
CCL2 3'UTR
Poly A
B
Relative luciferase activity (%)
100
80
60
40
20
0
control
rs13900 C
rs13900 T
*
*
C
Relative luciferase activity (%)
200
160
120
80
40
0
*
*
pLightswitch-C + + - -
pLightswitch-T - - + +
pCMV6-Entry + - + -
pCMV6-HuR - + - +
D
Relative luciferase activity (%)
140
100
60
20
0
*
*
pLightswitch-C + + - -
pLightswitch-T - - + +
cnt-siRNA + - + -
HuR-siRNA - + - +

Figure 7

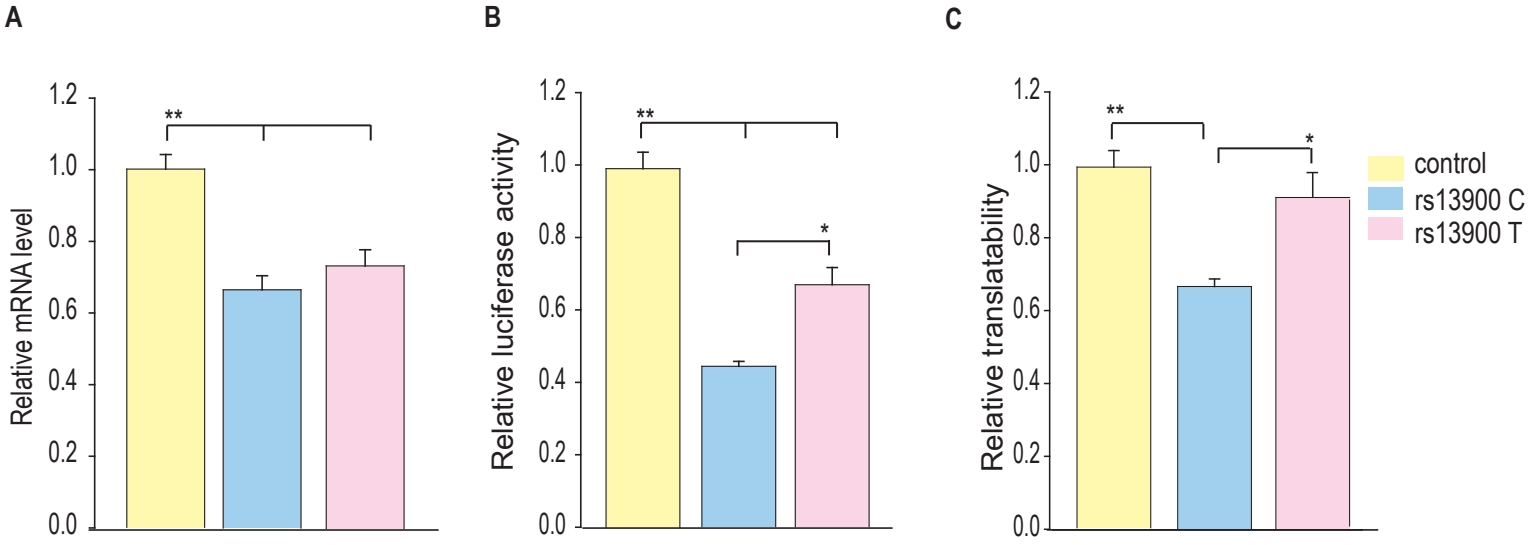
A
B
C
Relative mRNA level
Relative luciferase activity
Relative translatability
1.2
1.0
0.8
0.6
0.4
0.2
0.0
**
*
control
rs13900 C
rs13900 T

Figure 8

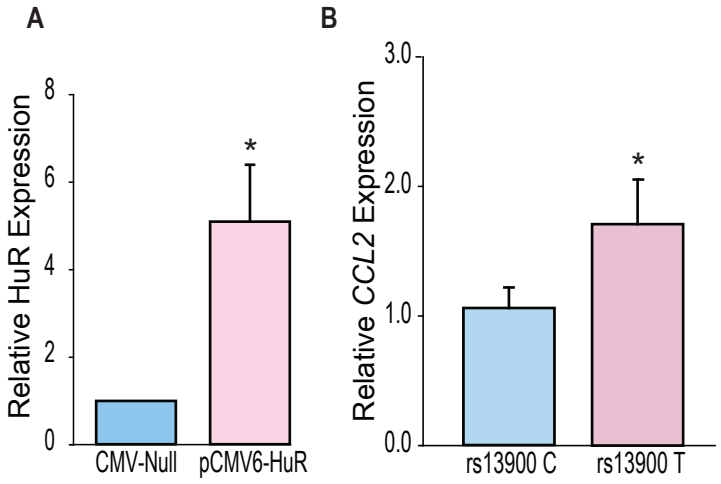
A
B
Relative HuR Expression
8
6
4
2
0
*
CMV-Null
pCMV6-HuR
Relative CCL2 Expression
3.0
2.0
1.0
0.0
*
rs13900 C
rs13900 T

Figure S1

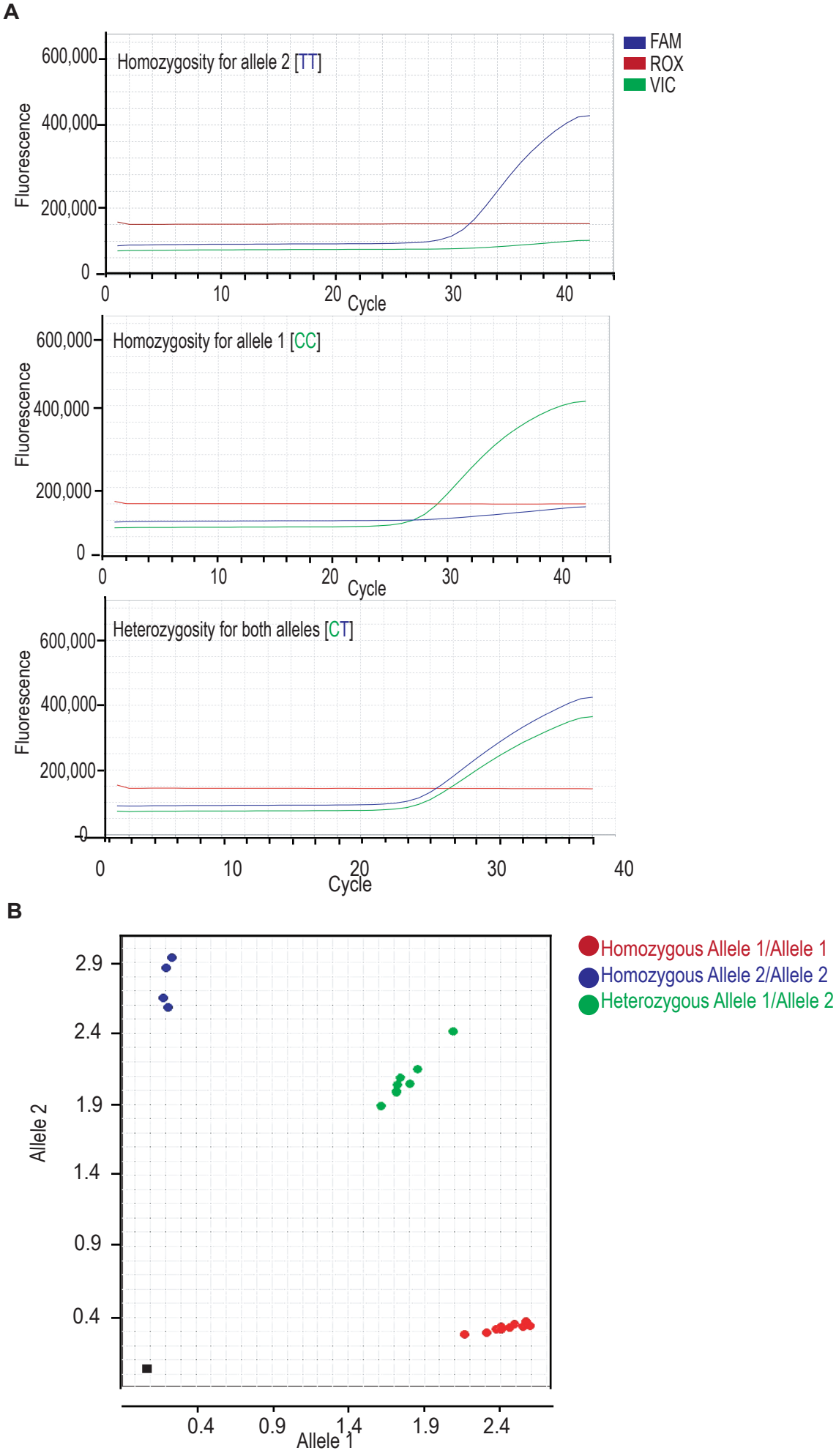
A
FAM
ROX
VIC
Homozygosity for allele 2 [TT]
Homozygosity for allele 1 [CC]
Heterozygosity for both alleles [CT]
Fluorescence
600,000
400,000
200,000
0
0
10
20
30
40
Cycle
B
Homozygous Allele 1/Allele 1
Homozygous Allele 2/Allele 2
Heterozygous Allele 1/Allele 2
Allele 2
2.9
2.4
1.9
1.4
0.9
0.4
Allele 1

Figure S2

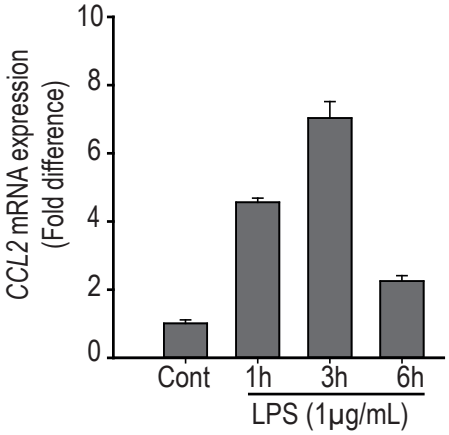
10
8
6
4
2
0
CCL2 mRNA expression
(Fold difference)
Cont
1h
3h
6h
LPS (1μg/mL)

Figure S3

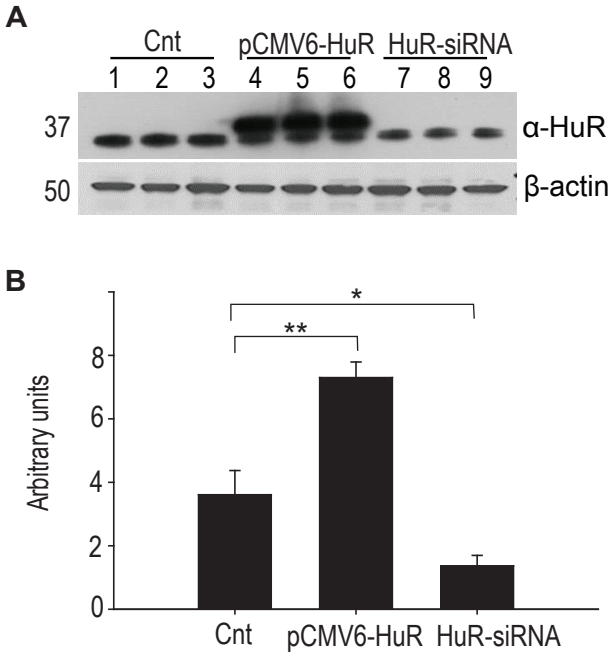
A
Cnt
pCMV6-HuR
HuR-siRNA
1 2 3 4 5 6 7 8 9
37
50
α-HuR
β-actin
B
Arbitrary units
0
2
4
6
8
*
**
Cnt
pCMV6-HuR
HuR-siRNA

Figure S4

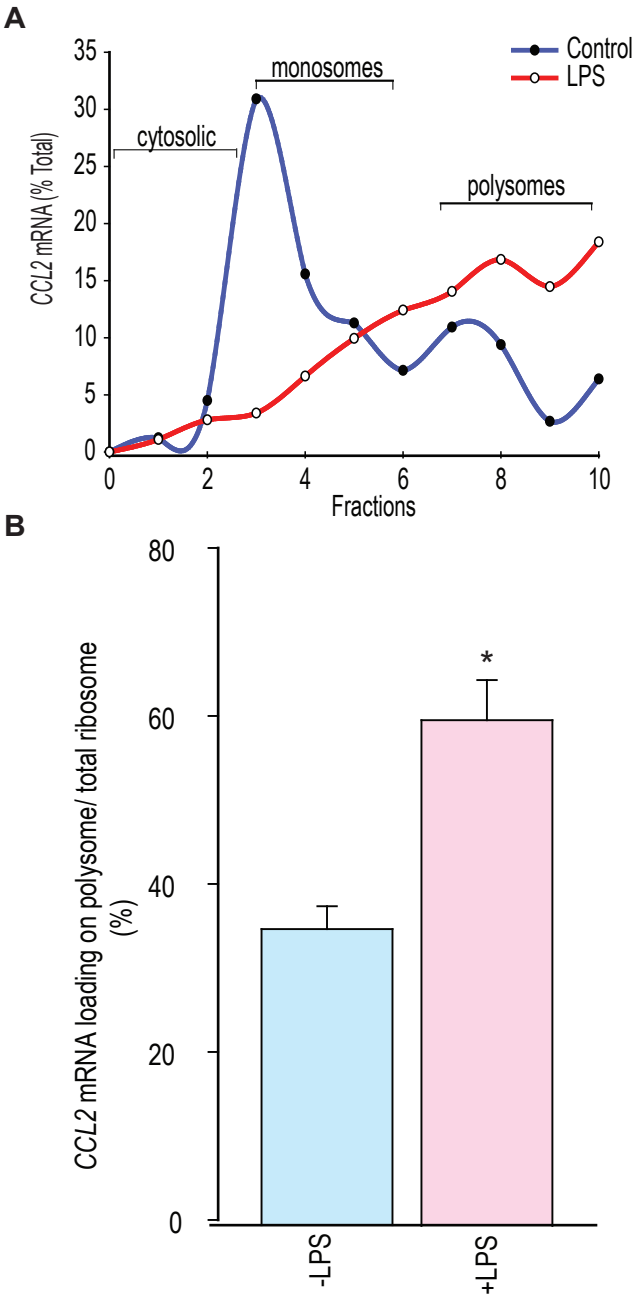
A
Control
LPS
monosomes
cytosolic
polysomes
CCL2 mRNA (% Total)
35
30
25
20
15
10
5
0
0
2
4
6
8
10
Fractions
B
CCL2 mRNA loading on polysome/ total ribosome (%)
80
60
40
20
0
*
-LPS
+LPS

Figure S5

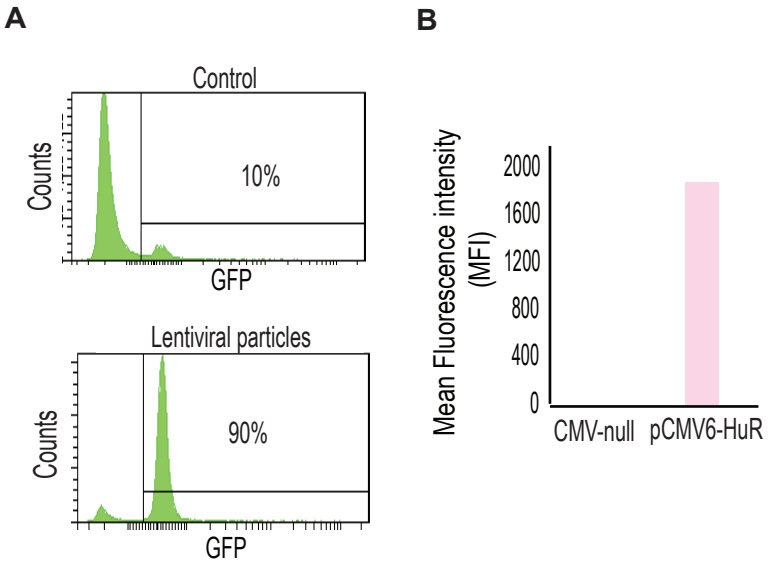
A
Control
Counts
10%
GFP
Lentiviral particles
Counts
90%
GFP
B
Mean Fluorescence intensity (MFI)
2000
1600
1200
800
400
0
CMV-null
pCMV6-HuR

Figure S6

A

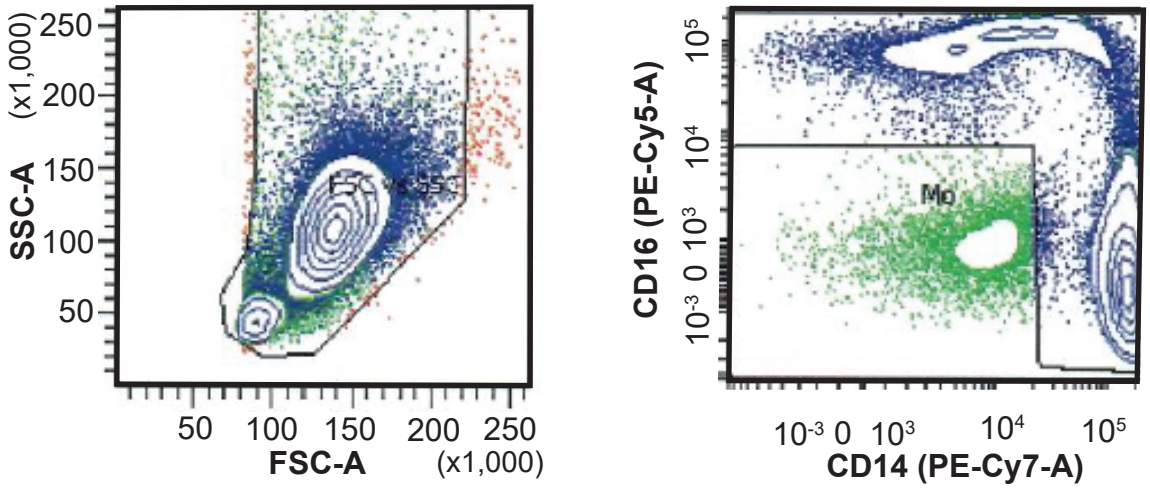
SSC-A (x1,000)
250
200
150
100
50
FSC-A (x1,000)
50 100 150 200 250
CD16 (PE-Cy5-A)
Mo
CD14 (PE-Cy7-A)

B

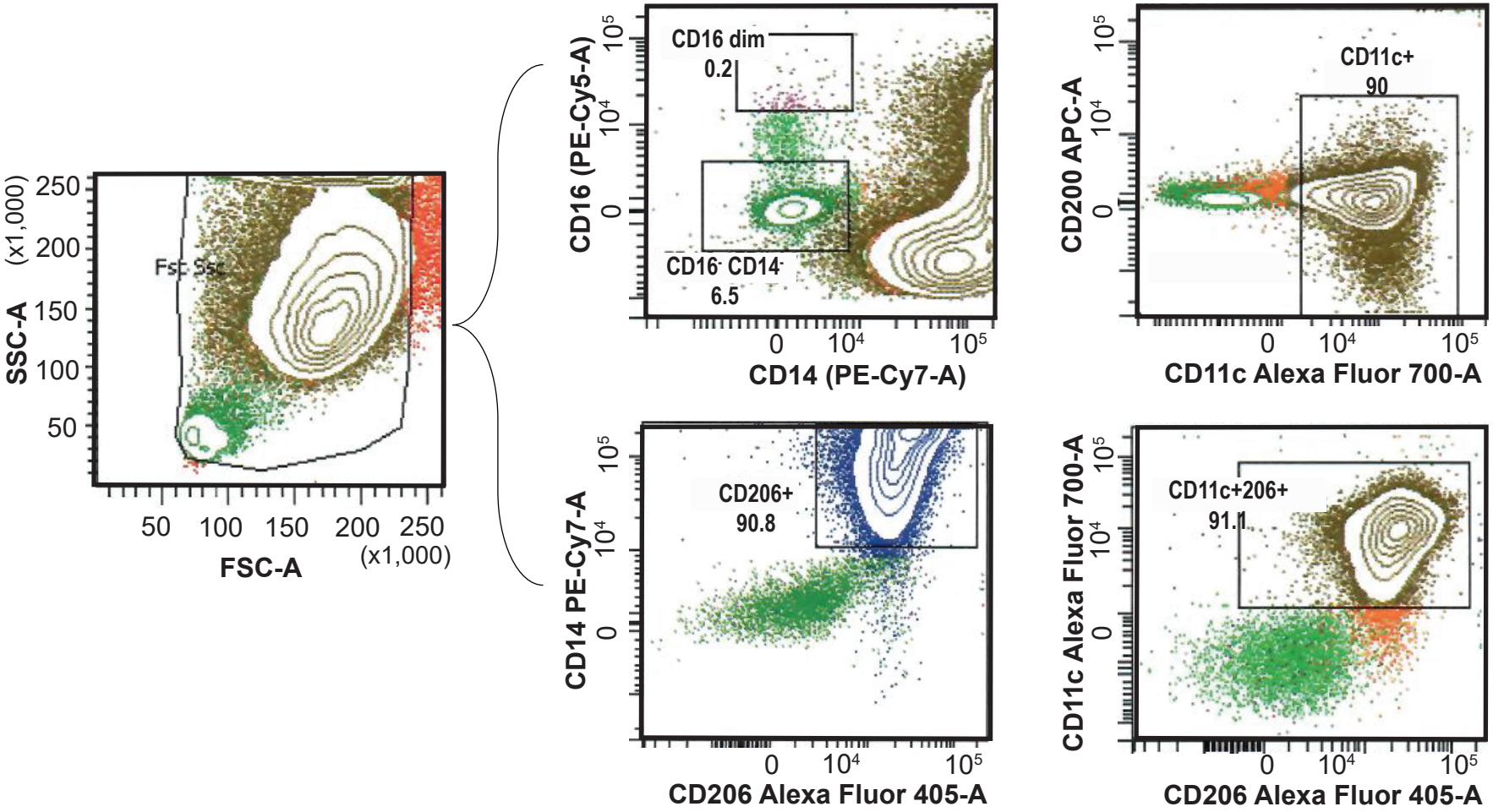
SSC-A (x1,000)
FSC-A (x1,000)
CD16 dim
0.2
CD16- CD14-
6.5
CD16 (PE-Cy5-A)
CD14 (PE-Cy7-A)
CD11c+
90
CD200 APC-A
CD11c Alexa Fluor 700-A
CD206+
90.8
CD14 PE-Cy7-A
CD206 Alexa Fluor 405-A
CD11c+206+
91.1
CD11c Alexa Fluor 700-A
CD206 Alexa Fluor 405-A

Figure S7

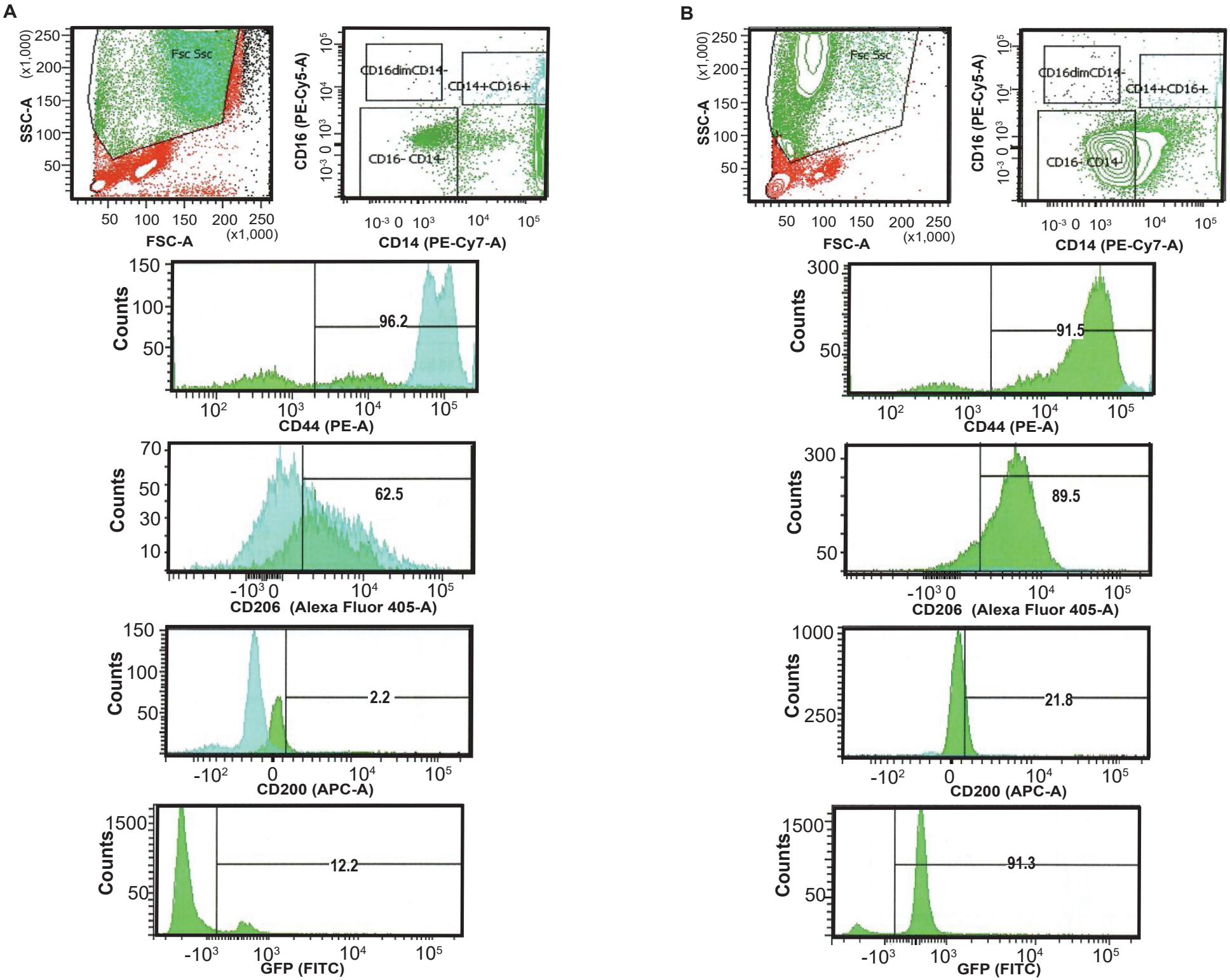
A
B
Fsc Ssc
SSC-A (x1,000)
FSC-A (x1,000)
CD16dimCD14-
CD14+CD16+
CD16- CD14-
CD16 (PE-Cy5-A)
CD14 (PE-Cy7-A)
Counts
96.2
CD44 (PE-A)
62.5
CD206 (Alexa Fluor 405-A)
2.2
CD200 (APC-A)
12.2
GFP (FITC)
91.5
89.5
21.8
91.3

	rs13900 (n=42)
Reference allele [CC]	18 (42.8%)
Heterozygous [CT]	16 (38.09%)
Alternative allele [TT]	8 (19.04%)
MAF	0.38
Heterozygosity	0.47
No of alleles	84
Hardy Weinberg *P*	0.459

Supplementary Table 1. Allele carriages and allele frequencies of rs13900 in healthy volunteers, MAF, minor allele frequency.

RBP	Tissue type	rs#	Position	Strand	CLIP-seq technology and peak calling method	Score	PhastCons score	PhyloP score	Data accession	Ref strand	Alt strand	SNP position
ELAVL1	HeLa	rs13900	chr17:34256881-34256901	+	PAR-CLIP,Piranha_0.01	11	0.024	0.227	GSE29943,GSM741175	C	T	chr17:34256891-34256892
ELAVL1	HeLa	rs181021073	chr17:34256857-34256876	+	PAR-CLIP,PARalyzer	0.647	0.002	0.14	GSE29943,GSM741173	T	G	chr17:34256868-34256869
ELAVL1	HeLa	rs181021073	chr17:34256857-34256876	+	PAR-CLIP,PARalyzer	0.653	0.002	0.14	GSE29943,GSM741174	T	G	chr17:34256868-34256869
ELAVL1	HeLa	NA	chr17:34257108-34257130	+	PAR-CLIP,PARalyzer	0.623	0.001	-0.256	GSE29943,GSM741173	AT	A	chr17:34257109-34257110
ELAVL1	HeLa	NA	chr17:34257101-34257121	+	PAR-CLIP,Piranha_0.01	9	0	-0.39	GSE29943,GSM741173	AT	A	chr17:34257109-34257110
ELAVL1	HeLa	NA	chr17:34257101-34257121	+	PAR-CLIP,Piranha_0.01	6	0	-0.39	GSE29943,GSM741175	AT	A	chr17:34257109-34257110

Supplementary Table 2. Crosslinking immunoprecipitation (CLIP) analysis of HuR binding sites on the 3'untranslated region (3'UTR) of the *CCL2* gene. Summary of the SNPs located within HuR-binding regions is shown including SNP ID (rs#), genomic coordinates, strand, binding score, conservation scores (PhastCons, PhyloP), dataset accession numbers, alleles, and SNP position within peak region. Data was generated using POSTAR3 using the variation module.

	gDNA	Cytosol	Monosome	Polysome
D-1	0.975806	0.872946	0.873425	1.778429
D-2	1.034091	1.557778	1.441919	1.562622

Supplementary Table 3. Loading of rs13900 alleles to cytosolic, monosomal and polysomal fractions from macrophage extracts prepared from heterozygous donors. T:C ratio > 1 indicates increased levels of the T allele relative to C allele.

S.N	Reagents	Source	Cat.No.	Note
1	rs13900 TaqMan Assay	ThermoFisher Scientific	4351379	C7449810_10*
2	QIAamp DNA Blood Mini Kit	Qiagen	51104	
3	TaqMan Genotyping Master Mix	ThermoFisher Scientific	4371355	
4	Histopaque-1077	Millipore Sigma	10771	
5	Lipopolysaccharides from *E.coli* 0:111:B4	Millipore Sigma	L2630	1µg/mL**
6	EasySep Human Monocyte Isolation Kit	StemCell Technologies	19359	
7	Recombinant Human M-CSF	Peprotech	300-25	50 ng/mL**
8	Pe-Cy 7 Mouse-Anti Human $CD14^+$	BD-Pharmigen	562698	
9	FITC Mouse- Anti Human CD64+	BD-Pharmigen	555522	
10	BV421 Mouse Anti-Human CD206+	BD-Pharmigen	564060	
11	AlexaFluor 700 Mouse-Anti Human $CD11c^+$	BD-Pharmigen	561352	
12	PE CY 5 Mouse Anti-Human CD16+	BD-Pharmigen	555408	
13	RNeasy Plus Mini kit	Qiagen	74134	
14	MultiScribe Reverse Transcriptase	ThermoFisher Scientific	4311235	
15	CCL2 TaqMan Gene Expression Assays	ThermoFisher Scientific	4331182	Hs00736046_m1*
16	18S TaqMan Gene Expression Assays	ThermoFisher Scientific	4331182	Hs03003631_g1*
17	Click-iT-Nascent RNA Kit	Invitrogen	C10365	
18	Actinomycin D	MilliporeSigma	A1410	
19	Superscript Vilo Kit	ThermoFisher Scientific	11754250	
20	AmpliTaq Gold 360 Master Mix	ThermoFisher Scientific	4398881	
21	GeneJET PCR Purification Kit	ThermoFisher Scientific	K0701	
22	ELAVL1 human recombinant protein	OriGene	TP301562	
23	HuR/ELAV1 Antibody	Santa Cruz	sc-5261	
24	hnRNP E1 Antibody (T-18)	Santa Cruz	sc-16504	
25	Normal Goat IgG	Santa Cruz	sc-2028	
26	β Actin Antibody (2A3)	Santa Cruz	sc-517582	
27	Goat Anti-Mouse IgG-HPR	Santa Cruz	sc-2005	
28	Lipofectamine 3000	ThermoFisher Scientific	L3000008	
29	RIPA Lysis and Extraction Buffer	ThermoFisher Scientific	89900	
30	Protease Inhibitor Cocktail Tablets	Millipore Sigma	11836170001	
31	Nitrocellulose Membranes	Thermo Scientific	88024	
32	RIP-Assay Kit	MBL Life science	RN1001	

Supplementary Table 4. Reagents used in the study with source and catalog numbers.

*Assay ID, ** Concentration used